T H E U N I V E R S I T Y O F T U L S A

THE GRADUATE SCHOOL

CHOKE MANAGEMENT OF UNCONVENTIONAL RESERVOIRS BY USE OF AN APPROXIMATE SEMIANALYTICAL MODEL

by
Yuanshan Zhang

A thesis submitted in partial fulfillment of

the requirements for the degree of Master of Science

in the Discipline of Petroleum Engineering

The Graduate School

The University of Tulsa

2017

T H E U N I V E R S I T Y O F T U L S A

THE GRADUATE SCHOOL

CHOKE MANAGEMENT OF UNCONVENTIONAL RESERVOIRS BY USE OF AN APPROXIMATE SEMIANALYTICAL MODEL

by
Yuanshan Zhang

A THESIS

APPROVED FOR THE DISCIPLINE OF

PETROLEUM ENGINEERING

By Thesis Committee

_____, Chair
Rami M. Younis

_____
Randy Hazlett

_____
Christian Constanda

ABSTRACT

Yuanshan Zhang (Master of Science in Petroleum Engineering)

Choke management of unconventional reservoirs by use of an approximate semianalytical model

Directed by Rami Younis

59, pp., Chapter 5: Conclusions

(259 words)

In the unconventional sector, inexpensive and quick interventions that lead to improvements in profitability are highly attractive. Choke-management is a prime target application area to introduce significant economic impact. In current engineering workflows, well control optimization is typically achieved by the application of an integrated reservoir modeling approach that is tied to a closed-loop reservoir management system. This approach requires considerable dedicated resources and may be time-consuming. Win this work, an approximate and rapid optimization system is developed to enable practical improved choke-management based on sound physics.

Multi-fractured horizontal wells (MFHWs) are the standard in completions technology for production from reservoirs with extremely low permeability. Generally, transient linear flow is the dominant flow regime for many MFHWs producing from gas and oil reservoirs with ultra-low permeability. In these reservoirs, this regime can last for several years before the appearance of a boundary dominated flow regime.

In this work, a semi-analytical model that is derived from a dynamic drainage

area (DDA) concept is applied in order to forecast production from MFHWs that are completed in liquid-rich low-permeability reservoirs exhibiting two-phase flow of gas- and oil-condensate.

The ensemble smoother with multiple data assimilation (ES-MDA) method is applied in order to assimilate dynamic production performance history. The calibrated model is used to evaluate an objective function that measure profitability. Optimal well controls are then obtained to maximize net present value (NPV). Based on the optimization results, a generalization of optimal choke-management strategies is proposed based upon the curvature of the vaporized oil gas ratio with respect to pressure for condensate gas cases.

ACKNOWLEDGEMENTS

First and foremost, I would like to express my sincere gratitude to my advisor, Dr. Rami M. Younis, for his unconditional support, patience, encouragement and guidance throughout my graduate education and research activities. Dr. Younis is very knowledgeable and a true expert in his field. He believed in me since the beginning and had devoted immeasurable amount of time and effort to cultivate my professional growth in petroleum engineering. I am truly inspired by all that he has done for me and I will always look up to him.

I would also like express my sincere appreciation to the other members of my thesis committee, Dr. Randy Hazlett and Dr. Christian Constanda, for their time and energy in serving on my committee and their insightful comments regarding my research. I am very grateful to have such knowledgeable and dedicated professors, who guided me and taught me so much as I complete my graduate degree.

I further owe my gratitude to the Department of Petroleum Engineering, including all the faculty and staff. I would also like to thank my friends and colleagues in TU for their company and moral support. In particular, I thank Jiamin Jiang, Ranran Lu, Guotong Ren and Reza Nia for their valuable time and utmost support throughout my work.

Lastly, I would like to express my deepest gratitude to my parents and my family for their endless love, support, and encouragement throughout my life. My achievements would not have been possible without their help and inspiration.

TABLE OF CONTENTS

LIST OF FIGURES

CHAPTER 1

INTRODUCTION

1.1 Literature Review

In recent years, due to the ever-increasing energy demand, the exploration of unconventional reservoirs with very low permeability (e.g. shale gas reservoirs) has received growing attention all over the world, especially in North America. To maximize the recovery of hydrocarbon liquids from tight/shale oil and liquid-rich shale gas reservoirs, multi-stage hydraulic fracturing technology combined with the use with horizontal wells has been applied, leading to economic development of such formations.

Given the focus of exploration on unconventional reservoir with multi-fractured horizontal wells (MFHWs), it is highly desirable to develop rigorous method capable of forecasting production rates. Such methods can then be used in characterization of reservoir rock and fluid properties by matching the production history. Also, they can also be used in choke management where production optimization is implemented to get the most desirable well schedule resulting in the maximum net present value (NPV).

One main productivity evaluation method is numerical simulation, which can accurately handle the highly nonlinear physical coupling, multi-phase flow behavior, and the complex fracture network with non-ideal fracture geometries (Olorode et al., 2013). Although numerical simulators are more rigorous and are able to capture physics in more detail, it needs significant time and data to set up. History matching and optimization are iterative processes, hence such applications based on numerical simulators are very time-

consuming. Also, in the early stages of exploration, numerical simulation has limited advantage due to lack of sufficient geological data. However, analytical models based on abstract physical models are much faster and can be practically accurate if the physics is included in the model carefully (Shojaei and Tajer 2013).

Several analytical productivity models have been proposed by researchers to predict production rates of MFHWs. Raghavan and Joshi (1993) assumed all production comes from the hydraulic fractures and the pressure drop within fractures are negligible. Based on that assumption, they suggested one analytical productivity model with the use of the effective wellbore radius concept combined with the superposition principle to calculate the productivity under steady-state conditions. Wei and Economides (2005) also assumed that the fluid production is only from fractures and there is no production directly from the matrix. They assumed that the flow from the matrix to the fracture is linear and the flow inside the fracture is both linear and radial. They used choke skin factor (Mukherjee and Economides, 1991) to model flow convergence. Guo et al. (2009) proposed another productivity model under pseudo-steady state. In their assumption, the flow in the non-stimulated reservoir is radial, the flow from the matrix to the fracture in the fractured region is linear and inside the fracture, the flow toward wellbore is a combination of linear and radial flow.

In addition to the analytical productivity index models mentioned in the previous paragraph, there are several analytical pressure transient models of a horizontal well with multiple uniformly-spaced transverse hydraulic fractures. Guo et al. (1994) characterized different flow regimes during pressure-transient analysis for both infinite and bounded single phase reservoirs, and then developed analytical solutions for both finite and

infinite conductivity using source functions and the superposition principle. Ozkan and Raghaven (1991) derived the point-source solution in the Laplace-transform domain. Based on that, Raghaven and Chen (1997) developed a more detailed model for transient behavior of MFHWs where skin factors are used to account for problems such as flow convergence toward the horizontal well. In their model, each fracture is assumed to have distinct properties and fracture spacing can also be different. Brown et al. (2011) presented an analytical trilinear flow solution which couples linear flows in three contiguous flow regions with distinct properties: the outer reservoir (beyond the hydraulic fracture tips), the inner reservoir (between fractures) and the hydraulic fractures.

Note that, MFHWs producing from gas condensate and volatile oil reservoirs generally present long transient flow periods, during which two phase flow of gas and condensate or gas and oil begins when the reservoir pressure drops below the dew point/ bubble point pressure. However, the analytical methods mentioned above have been primarily developed only for single phase flow. These method are not yet able to handle the complex two phase flow for tight oil and liquid-rich gas reservoirs flowing below the saturation pressure. In this work, a novel and rigorous semi-analytical method for flow-rate forecasting proposed by Clarkson and Qanbari (2016) is implemented for history matching and production optimization, as a practical alternative to numerical simulation for tight gas condensate and oil reservoirs experiencing two phase flow during the transient flow period. This approximate analytical method derived from dynamic-drainage-area concept is discussed in detail later in chapter 2.

The geological and petrophysical properties used in the model (either analytical or

numerical) which are estimated using data from well testing, logs, cores, etc., do not reveal the actual reservoir. Hence, the result of the model may differ from the observation data in reality. Forecasting based on this result would be completely wrong. To minimize this difference between predicted performance and the actual production data, a history matching process is required.

The geological model parameters are put into the model first to calculate the production performance. After producing for a while, the production history (e.g. pressure, production rate/total, gas-oil ratio) can be used to compare with the observed data (true data) to better constrain the model parameters. The model parameters are then modified in such a way that the forecasting data matches with the actual observed data. This data assimilation process is called history matching. In early time, history matching is conducted manually by trial and error. This makes the process very time-consuming. Another more efficient process is automatic history matching. Consider a reservoir simulation process as a forward model where model parameters are given as inputs to forecast production performance. The history matching process is thus an inverse problem, where we use the production history to get model parameters. Therefore, a more rigorous history matching process is developed by solving a specific inverse problem mathematically through the minimization of an objective function.

Following Sarma et al. (2007), history matching algorithms can be categorized to three general classes: stochastic algorithms, gradient-based methods, and Kalman filter approaches. Stochastic global search techniques include genetic algorithms (Erbas and Christie, 2007), simulated annealing (Ouenes, 1993), Tabu search (Yang et al., 2007), neighborhood algorithms (Sambridge, 1999; Nicotra et al., 2005). Stochastic algorithms

treat the simulator as a black box and are straightforward to implement and tend to avoid local minima. But they usually require numerous simulations for convergence, resulting in inefficiency.

The gradient-based method is one of the most efficient history matching methods. Initially, Chen et al. (1974) and Chavent et al. (1975) used the adjoint method to calculate the gradient of the objective function and then applied first order gradient-based optimization algorithms to get minimum for single-phase flow problem. Other researchers (Wasserman et al., 1975; Lee and Seinfield 1987; Zhang and Reynolds 2002) have modified and extended the application for multiphase flow with the adjoint method. Another gradient-based approach is to calculate the gradients of all observed data with respect to model parameters to develop the Hessian matrix. The Hessian is used in second order optimization algorithms, such as Gauss-Newton. The advantage of the gradient-based method is that it is fast and efficient with adequate gradient. The disadvantage is that it is not independent of reservoir simulators, which is to say, the Jacobian matrix is needed to calculate the gradient, making it very complicated to solve for large-scale problems.

The ensemble Kalman filter (EnKF) was originally introduced to petroleum science by Evensen (1994) as a sequential data assimilation algorithm. The EnKF is based on the Kalman filter which estimates the state of a linear dynamical system from a series of noisy measurements. In this approach, errors are represented by an ensemble of realizations. To use the sequential data assimilation characteristic of EnKF, the history matching problem has to be modified from a parameter estimation problem to a parameter state estimation problem. It is computationally efficient, easy to implement

and it does not require adjoint implementation for gradient computation. However, its application to history match field cases often fails to provide a reasonable characterization of uncertainty. In this work, we used the ensemble smoother with multiple data assimilation (ES-MDA) method developed by Emerick and Reynolds (2013) to history match the model parameters. The algorithm is described in detail in chapter 3.

Lastly, production optimization followed by history matching is implemented to get the optimal well control corresponding to the maximum net present value (NPV) of production from the reservoir. Gradient-based optimization algorithms include 1) steepest descent, 2) conjugate gradient, 3) Newton, 4) Quasi-Newton, and 5) trust-region.

The steepest descent method is a first order iterative algorithm which uses the gradient vector at each point as the search direction for each iteration. The search direction is

$$\boldsymbol{P}_k = -\nabla \boldsymbol{f}(\boldsymbol{x}_k). \tag{1.1}$$

The conjugate gradient method is another line search algorithm where the search direction $\boldsymbol{P}_k$ is a linear combination of the steepest descent direction $\nabla \boldsymbol{f}(\boldsymbol{x}_k)$ and the previous conjugate gradient direction,

$$\boldsymbol{P}_k = -\nabla \boldsymbol{f}(\boldsymbol{x}_k) + \beta_k \boldsymbol{P}_{K-1}. \tag{1.2}$$

While the two methods mentioned above only require the gradient, Newton's method, which uses a second-order Taylor series expansion of the objective function, requires calculation of both the gradient and the Hessian matrix. The search direction of Newton's method is defined as

$$\boldsymbol{P}_k = -\mathbf{H}^{-1}(\boldsymbol{x}_k)\nabla \boldsymbol{f}(\boldsymbol{x}_k). \tag{1.2}$$

In place of the true Hessian matrix, $\mathbf{H} = \nabla^2 \boldsymbol{f}(\boldsymbol{x}_k)$, the Quasi-Newton method only requires the gradient information to construct an approximate Hessian, $\mathbf{B}_k$. Thus the search direction is

$$\boldsymbol{P}_k = -\mathbf{B}^{-1}(\boldsymbol{x}_k)\nabla \boldsymbol{f}(\boldsymbol{x}_k). \tag{1.2}$$

By measuring the changes in gradients, the approximate Hessian is constructed by updates through iterations. Two popular quasi-Newton methods are the Broyden-Fletcher-Goldfarb-Shanno (BFGS) method and the Davidon-Fletcher-Powell (DFP) method.

The above line search methods use the quadratic model of the objective function to generate search direction, and then find the step-size. Another fundamental strategy is the trust region method. Trust region methods define a region around the current iterate, within which they "trust" the model (usually a quadratic model) to resemble the objective function, then, they find the approximate minimizer of the quadratic function. These methods choose the direction and step size simultaneously.

1.2 Outline

There are five chapters in this thesis. Chapter 2 describes a semi-analytical model based on the dynamic-drainage-area theory used in this work, followed by the correlations for the input property package (e.g. PVT properties). Then, the forecasting result is compared with the results of the numerical simulations through Eclipse (E100). Chapter 3 focuses on describing the ES-MDA method we used to history match the petrophysical parameters. After we have the history-matched forward model, production optimization is introduced in chapter 4 to get the optimal well control which gives us the maximum net present value. Last, chapter 5 concludes the thesis with a summary of accomplishments and recommendations for future work.

CHAPTER 2

APPROXIMATE SEMIANALYTICAL MODEL

Multi-fractured horizontal wells (MFHWs) are efficient to improve the productivity of reservoirs with extremely low permeability. Generally, transient linear flow is the dominate flow regime for many MFHWs producing from gas and oil reservoirs with ultra-low permeability, which can last for several years before encountering the boundary dominant flow regime.

The distance-of-investigation (DOI) concept is used to estimate dynamic drainage area (DDA) to predict production from tight gas condensate and oil reservoirs. At each time step, a multiphase version of linear-flow productivity index (PI) equation is coupled with material balance equations for gas, condensate or oil to solve for pressure, saturation and flow rates (which is embedded in the DOI calculation) iteratively. This chapter focuses on describing the theory of an approximate semi-analytical model derived from the DDA concept (Clarkson et al. 2015). Validation with numerical simulation is carried out afterwards.

2.1 Theory and Method

Clarkson and Qanbari (2016) developed an approximate semi-analytical method for forecasting gas condensate and oil wells in tight reservoirs. Here, linear flow geometry is assumed in both primary hydraulic fracture and non-stimulated region. The DOI as a function of time is used to describe pressure propagation from fractures. It can

be interpreted into an "area of investigation" at each time step during transient flow. The DDA concept is exemplified in Figure (2.1) for a linear-flow scheme. In Figure (2.1), $\bar{p}_{inv}$ is the average pressure in the investigated area and $\bar{S}_{o,inv}$ is the average oil saturation in the investigated area. Consider the pressure propagation at two different time steps, Timestep 1 and Timestep 2. At Timestep 1, the distance of the pressure front from the fracture is y_{inv1}. The inflow and material balance equations are solved iteratively for average pressure, average saturation and flow rates within the investigated area. At Timestep 2, the distance of the pressure front from the fracture increases to y_{inv2} and calculations are repeated. After calculating the distance of investigation, a time-dependent linear productivity index (PI) equation for multiphase flow is used to compute the fluid production rate.

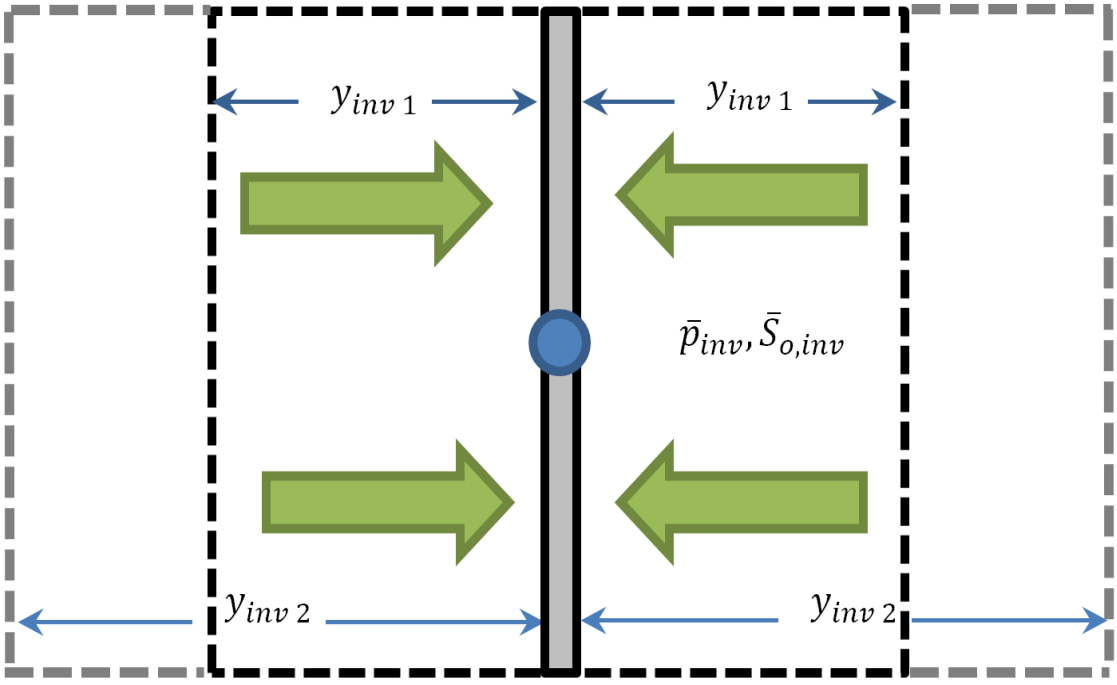

Figure 2.1 Distance of investigation at two different times, based on dynamic drainage area concept.

During transient linear flow, at each time step, the oil/condensate production rate under constant-flowing-rate condition is

$$q_o = \frac{k_i h[m_o(\bar{p}_{inv}) - m_o(p_{wf})]}{141.2\mu_{oi}B_{oi}\left[\frac{2}{\pi}\left(\frac{y_{inv}}{x_{ft}}\right)\right]} + \frac{R_v(\bar{p}_{inv})}{1000}\frac{k_i h[m_g(\bar{p}_{inv}) - m_g(p_{wf})]}{1424T\left[\frac{2}{\pi}\left(\frac{y_{inv}}{x_{ft}}\right)\right]} \quad (2.1)$$

and the gas production rate is

$$q_g = \frac{k_i h[m_g(\bar{p}_{inv}) - m_g(p_{wf})]}{1424T\left[\frac{2}{\pi}\left(\frac{y_{inv}}{x_{ft}}\right)\right]} + \frac{R_s(\bar{p}_{inv})}{1000}\frac{k_i h[m_o(\bar{p}_{inv}) - m_o(p_{wf})]}{141.2\mu_i B_{oi}\left[\frac{2}{\pi}\left(\frac{y_{inv}}{x_{ft}}\right)\right]}, \quad (2.2)$$

where q_o is oil/condensate production rate, q_o is gas production rate, k_i is the absolute permeability at initial reservoir pressure, h is reservoir thickness, μ_{oi} is oil viscosity at initial reservoir pressure, B_{oi} is oil viscosity at initial reservoir pressure, y_{inv} is radius of the distance of investigation (DOI), x_{ft} is total fracture half-length, T is reservoir temperature, m_o is oil pseudopressure, m_g is gas pseudopressure, R_v is vaporized oil-gas ratio, R_s is solution gas-oil ratio and $\bar{p}_{inv}$ is the average pressure in the area of investigation.

In Eq. (2.1), the first term on the right-hand side stands for the flow of free oil (oil in place), while the second term accounts for the flow vaporized condensate. 141.2 comes from the unit conversion between field unit and SI unit for oil, and 1424 corresponds to gas.

The radius of the investigation (ROI) or distance of investigation (DOI),

$$y_{inv} = \begin{cases} 0.159\sqrt{\frac{k_i}{\emptyset_i \mu_{oi} c_{ti}}} & \text{oil reservoir} \\ 0.159\sqrt{\frac{k_i}{\emptyset_i \mu_{gi} c_{ti}}} & \text{gas reservoir,} \end{cases} \quad (2.3)$$

where c_{ti} is the total compressibility at initial reservoir pressure and t is time. As simulation time increases, the pressure propagation gradually reaches the boundary. For

boundary-dominated-flow period, y_{inv} remains constant and equals to fracture half-distance, y_e.

By introducing the concept of pseudo-pressures of oil and gas, reservoir properties like relative permeability, along with fluid properties such as gas compressibility and gas viscosity, which are pressure-dependent variables, are taken into account. The pseudo-pressures of oil and gas are

$$m_o(p) = \frac{\mu_{oi}B_{oi}}{k_i}\int_{p_o}^{p}\frac{k(\hat{p})k_{ro}(S_o)}{\mu_o(\hat{p})B_o(\hat{p})}d\hat{p} \tag{2.4}$$

and

$$m_g(p) = \frac{2}{k_i}\int_{p_o}^{p}\frac{k(\hat{p})k_{rg}(S_o)\,\hat{p}}{\mu_g(\hat{p})Z_g(\hat{p})}\left[1+\frac{0.0031(\gamma_{API}-5.9)}{\gamma_{API}+131.5}R_v(p)\right]d\hat{p}. \tag{2.5}$$

The right hand side term in the brackets in Eq. (2.5) is used to convert the wet-gas volume factor to dry-gas volume factor (Whitson and Brule 2000).

Relative permeabilities of oil, k_{ro}, and gas, k_{rg}, are functions of saturation and do not directly relate to pressure. To evaluate the intergral part of Eqs. (2.4) and (2.5), a relation between oil saturation and pressure is needed. Qanbari and Clarkson (2013b) showed during the transient linear flow period, oil saturation and pressure have a stable relation. In other words, the production history does not affect the oil saturation-pressure relation. Clarkson and Qanbari (2016) proposed an empirical correlation between the oil saturation and pressure during the transient flow. In this correlation, the base oil saturation is calculated as a function of pressure for a reservoir with either black oil or gas condensate fluid, and then, another correlation is used to correct the base oil saturation value regarding to the effects of relative permeability and degree of under-saturation.

For oil reservoirs, the saturation,

$$S_{o,base}(p) = \frac{5.615B_o(p)}{5.615B_o(p)+B_g(p)\left(R_{sb}-R_s(p)\right)}, \tag{2.6}$$

where R_{sb} is the solution gas-oil ratio at bubble point pressure, B_o, B_g, R_s are functions of pressure and 5.615 comes from the unit conversion of B_o from rb/stb to rcf/stb. Due to the effect of relative permeability, Eq. (2.7) corrects the base saturation value calculated from Eq. (2.6) for the oil reservoir,

$$S_o(p) = 1 - \frac{S_{g,base}(p)}{1+\left(\frac{dk_{rg}}{dp}\right)_{S_{g,base}(p)}}. \tag{2.7}$$

For condensate gas reservoirs, saturation/pressure relationship is

$$S_{o,base}(p) = 5.615\left(\frac{R_{v,dew}-R_v(p)}{10^6-R_s(p)R_v(p)}\right)\frac{B_o(p)}{B_{gd,dew}(p)}, \tag{2.8}$$

where $R_{v,dew}$ is the vaporized condensate gas ratio (CGR) at dew point pressure and $B_{gd,dew}$ is the gas FVF at dew point pressure. Note that before reservoir pressure drops below dew point pressure, since there is no condensate drop out from the reservoir, $S_{o,base}$ is constant and equal to zero. Additionally for gas condensate reservoirs, the departure of the initial pressure from the saturation pressure should also be taken into account for gas reservoirs because of high compressibility of gas. Eq. (2.9) corrects the base saturation value calculated from Eq. (2.8) for a condensate gas reservoir:

$$S_o(p) = \frac{S_{o,base}(p)}{(1+(K_{ro})_{S_{o,base}}}\frac{p_i}{Z_{gi}}\frac{Z_g(p_d)}{p_d} \times \frac{1}{erfc^{-1}(\frac{p_i-p_d}{p_i})}, \tag{2.9}$$

where Z_g is the gas compressibility.

At time t, the total oil production, $N_p + q_o\Delta t$, is equal to the deference between the initial oil in-place and the current oil in-place at t, thus the material balance for the oil phase is

$$N_p + q_o \Delta t =$$

$$4x_{ft} y_{inv} h \left(\frac{\phi_i S_{oi}}{5.615 B_{oi}} + R_{vi} \frac{\emptyset_i S_{gi}}{10^6 B_{gdi}} - \frac{\phi(\bar{p}_{inv}) \bar{S}_{o,inv}}{5.615 B_o(\bar{p}_{inv})} - R_v(\bar{p}_{inv}) \frac{\phi(\bar{p}_{inv}) \bar{S}_{g,inv}}{5.615 B_o(\bar{p}_{inv})} \right), \quad (2.10)$$

where N_p is the cumulative oil production total from the previous time steps, q_o is the oil production rate at time t, $4x_{ft} y_{inv} h$ is the investigation area, and $\bar{S}_{o,inv}$ is the average oil/condensate saturation in the area of investigation. The first two terms in the bracket denote the original oil in-place (OOIP) and the initial amount of gas condensate while the last two terms in the bracket correspond to those of current time step. Similarly for gas phase,

$$G_p + q_g \Delta t = \frac{4x_{ft} y_{inv} h}{1000} \left(\frac{\emptyset_i S_{gi}}{B_{gdi}} + R_{si} \frac{\emptyset_i S_{oi}}{5.615 B_{oi}} - \frac{\phi(\bar{p}_{inv}) \bar{S}_{g,inv}}{B_{gd}(\bar{p}_{inv})} - R_s(\bar{p}_{inv}) \frac{\phi(\bar{p}_{inv}) \bar{S}_{o,inv}}{5.615 B_o(\bar{p}_{inv})} \right), \quad (2.11)$$

where G_p is the cumulative gas production total from the previous time steps, q_g is the gas production rate at time t, $4x_{ft} y_{inv} h$ is the investigation area, the first two terms in the bracket denote the original gas in-place (OGIP) and the initial amount of dissolved gas, and the last two terms in the bracket correspond to those of current time step.

In the material balance equations, average pressure in the area of investigation is needed to calculate the flow rates, as well as the cumulative production of previous time steps. Therefore, flow rate equations and material balance equations are coupled together to solve for q_g, q_o, $\bar{p}_{inv}$, and $\bar{S}_{o,inv}$ simultaneously at each time step. To do so, we substitute the equations for oil and gas flow rates, Eqs. (2.1) and (2.2), into the material balance equations, Eq. (2.10) and Eq. (2.11), which gives us two sets of non-linear equations with two unknowns, $\bar{p}_{inv}$ and $\bar{S}_{o,inv}$. The Newton-Raphson scheme is implemented to iteratively solve this non-linear system of equations. Given an initial

guess of average pressure, $\bar{p}_{inv}$, flow rates are calculated by Eqs. (2.1) and (2.2). Then we use material balance equations to update $\bar{p}_{inv}$.

2.2 Rock and Fluid Properties

In this section, we discuss in detail, the correlations we use to approximate the rock and fluid properties.

2.2.1 Rock properties

The permeability is assumed to be isotropic and constant. Porosity, which is a function of pressure, is defined as

$$\phi = \phi^0(x)\big(1 + x(p_0) + 0.5x^2(p_0)\big), \tag{2.12}$$

where

$$x(p_0) = C_r(p_0 - p^o_{rock}).$$

C_r is compressibility in $1/psi$, p^o_{rock} is reference pressure, and $\phi^0(x)$ is the homogeneous porosity field at reference pressure.

2.2.2 Rock-Fluid properties

In this study, Corey's model is implemented to generate two-phase relative permeability model:

$$k_{ro} = k^o_{ro}(S^*_o)^{n_o} \tag{2.13}$$

and

$$k_{rg} = k^o_{rg}(1 - S^*_o)^{n_g}, \tag{2.14}$$

where $k^o_{ro} = k_{ro}\big(S_o = 1 - S_{gc}\big)$ is the maximum relative permeability of oil, k^o_{rg} is the

maximum relative permeability of gas, the exponents n_o and n_g range from 1 to 6, and the normalized oil saturation is defined as

$$S_o^* = \frac{S_o - S_{or}}{1 - S_{or} - S_{gc}}.$$

2.2.3 Gas properties

Gas formation volume factor (FVF) is defined as follows:

$$B_g = 0.0282793 \frac{zT}{p} \left(\frac{rcf}{scf}\right), \tag{2.15}$$

where z is the gas compressibility factor, T is the temperature in ranking ($°R$), the pressure is in psia.

Lee et al. correlation is used for gas viscosity calculation:

$$\mu_g = k \times 10^{-4} \exp\left\{x \left(0.0433\, \gamma_{gf} \frac{p}{z(T+460)}\right)^y\right\}, \tag{2.16}$$

where,

$$k = \frac{(9.4 + 0.02Ma)(T+460)^{1.5}}{209 + 19Ma + (T+460)},$$

$$x = 3.5 + \frac{986}{T+460} + 0.01Ma,$$

$$y = 2.4 - 0.2x,$$

where γ_{gf} is the gas specific gravity, M_a is molecular weight of the gas.

We use an exponential function to approximate vaporized oil-gas ratio:

$$R_v = C_1 e^{C2*x}, \tag{2.17}$$

2.2.4 Oil properties

Following Vasquez and Beggs (1980) correlation, the oil formation volume factor for gas saturated (phase pressure below bubble point pressure) is given as follows:

$$B_o = 1 + C_1 R_s + C_2(T - 60)\left(\frac{\gamma_o}{\gamma_g}\right) + C_3 R_s(T - 60)\left(\frac{\gamma_o}{\gamma_g}\right), \quad (2.18)$$

where γ_o is the API gravity of oil, γ_g is the specific gas gravity, temperature T is in Fahrenheit ($^\circ F$). C_1, C_2, C_3 are coefficients (For $\gamma_o \leq 30^\circ API$, $C_1 = 4.677 \times 10^{-4}$, $C_2 = 1.751 \times 10^{-5}$, $C_3 = -1.811 \times 10^{-8}$; For $\gamma_o > 30^\circ API$, $C_1 = 4.670 \times 10^{-4}$, $C_2 = 1.100 \times 10^{-5}$, $C_3 = 1.377 \times 10^{-9}$). And for undersaturated oil (phase pressure below bubble point pressure) we have:

$$B_o = B_{ob} \exp\left(C_0(p_{bp} - p)\right), \quad (2.19)$$

where p_{bp} is bubble point pressure, B_{ob} denotes the oil FVF at p_{bp}.

Solution gas oil ratio is

$$R_s = C_1 \gamma_g p^{C_2} \exp\left(C_3\left(\frac{\gamma_o}{T+460}\right)\right), \quad (2.20)$$

where C_1, C_2, C_3 are coefficients (For $\gamma_o \leq 30^\circ API$, $C_1 = 0.0362$, $C_2 = 1.0937$, $C_3 = 25.7240$; For $\gamma_o > 30^\circ API$, $C_1 = 0.0178$, $C_2 = 1.1870$, $C_3 = 23.9310$).

Following Beggs and Robinson (1975) correlation, viscosity of dead oil (μ_{od}) is

$$\mu_{od} = 10^x - 1, \quad (2.21)$$

where

$$x = \frac{10^{(3.0324 - 0.02023 \times API)}}{T^{1.163}}. \quad (2.22)$$

Based on dead oil viscosity, the saturated oil viscosity (μ_{ol}) is

$$\mu_{ol} = [10.715(R_s + 100)^{-0.515}]\mu_{od}^b, \quad (2.23)$$

where

$$b = 5.44(R_s + 150)^{-0.338}. \quad (2.24)$$

We use Vasquez and Beggs (1980) correlation to calculate undersaturated oil viscosity

$$\mu_o = \mu_{ob}\left(\frac{p}{p_b}\right)^m, \quad (2.25)$$

where

$$m = 2.6p^{1.187}\exp(-11.513 - 8.98 \times 10^{-5}p). \quad (2.26)$$

2.3 Model Validation

In the following section, a numerical simulation carried out by Eclipse E100 is compared with the proposed semi-analytical solution to evaluate the accuracy of the saturation/pressure relationship as well as the new forecasting methodology. Then we investigate several cases with varying flowing pressure in systems with either oil or gas as the primary phase.

We assume that all hydraulic fractures are identical in the numerical model and we refine the cells around each fracture parallel to the fracture. The grid sizes increase geometrically as we get far from the fracture. In this way we can model the flow in this zone accurately. Figure 2.2 represents the base geometry used in our numerical model.

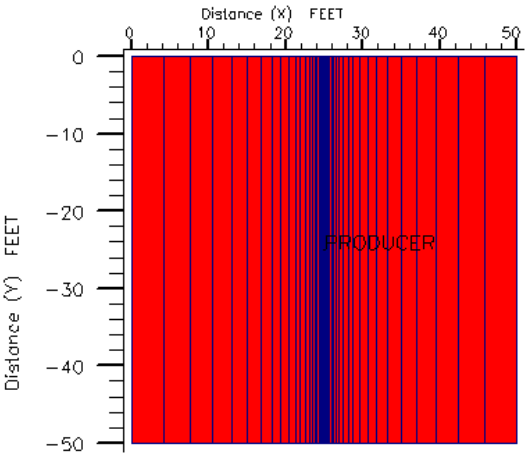

Figure 2.2. Base geometry with grid refinement around a fracture.

Case 1 is a gas condensate reservoir with a constant flowing pressure of 1000 psi and static absolute permeability of 0.005 md. The reservoir size is 20000 ft × 200 ft × 50

ft. It is producing from a horizontal well intercepted by ten fractures with the total fracture half- length of 1000 ft. Initially it is a single phase gas reservoir with the porosity of 0.08. The initial reservoir pressure is 6000 psi, and the dew point pressure is 3000 psi. Reservoir temperature is 250 $°F$. Figures 2.3 and 2.4 show the PVT properties of oil and gas respectively and Figure 2.5 corresponds to relative permeability curve.

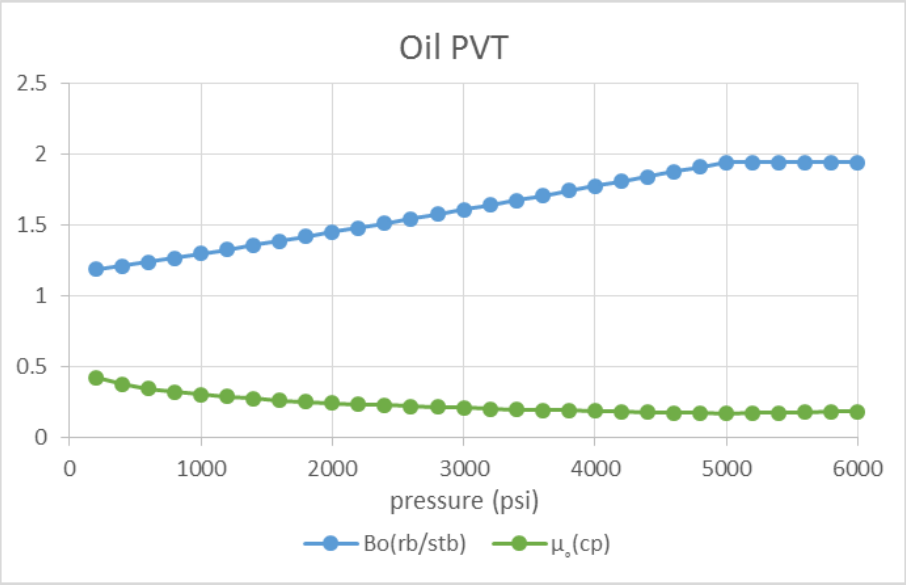

Figure 2.3. Oil PVT properties for case 1.

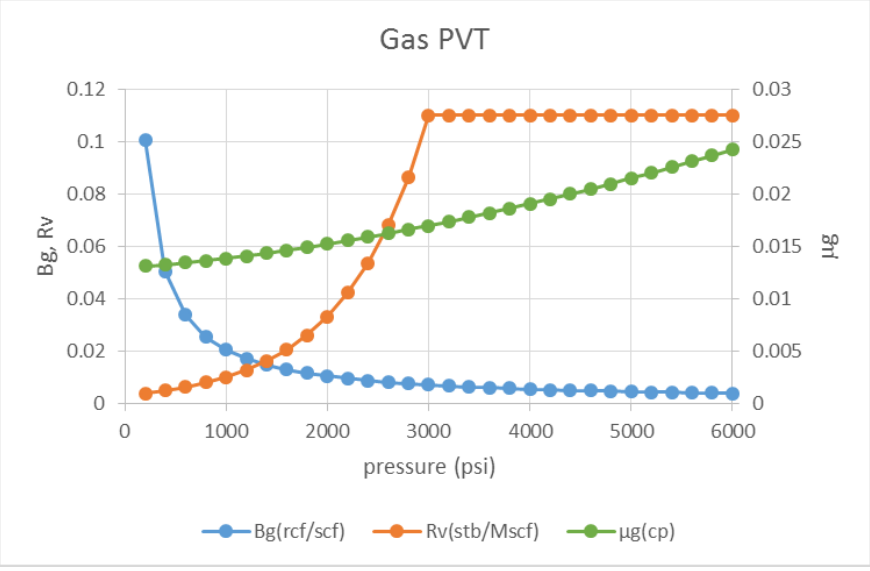

Figure 2.4. Gas PVT properties for case 1.

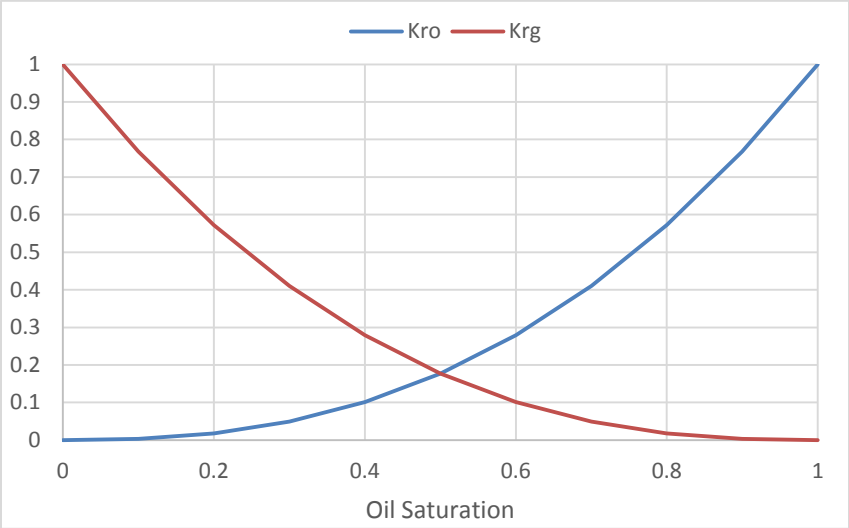

Figure 2.5. Relative permeability curves of oil and gas for case 1.

Figures. 2.6 and 2.7 compare the results from the analytical forecast methodology with the results of a two phase gas condensate case from ECLIPSE. As shown in Figure 2.6 both condensate and gas production rates have (-0.5) slope on a log-log plot. The flow rate results from the analytical model match the results obtained from the simulator. There is a minor mismatch for condensate at early times during transient-linear flow. As shown in Figure 2.7, the analytical method over estimates the cumulative production. However, the cumulative production from the analytical model is acceptable within engineering error (less than 10%). Final cumulative gas from the analytical forecasting method is 319 MMscf vs. 289 MMscf from the numerical simulation; final cumulative condensate production from the analytical forecasting method and the numerical simulation are, respectively, 3.29 MSTB (thousand STB) and 3.11 MSTB. The relative errors between the two approaches for forecasting cumulative gas and oil rate are respectively 9.4% and 5.47%.

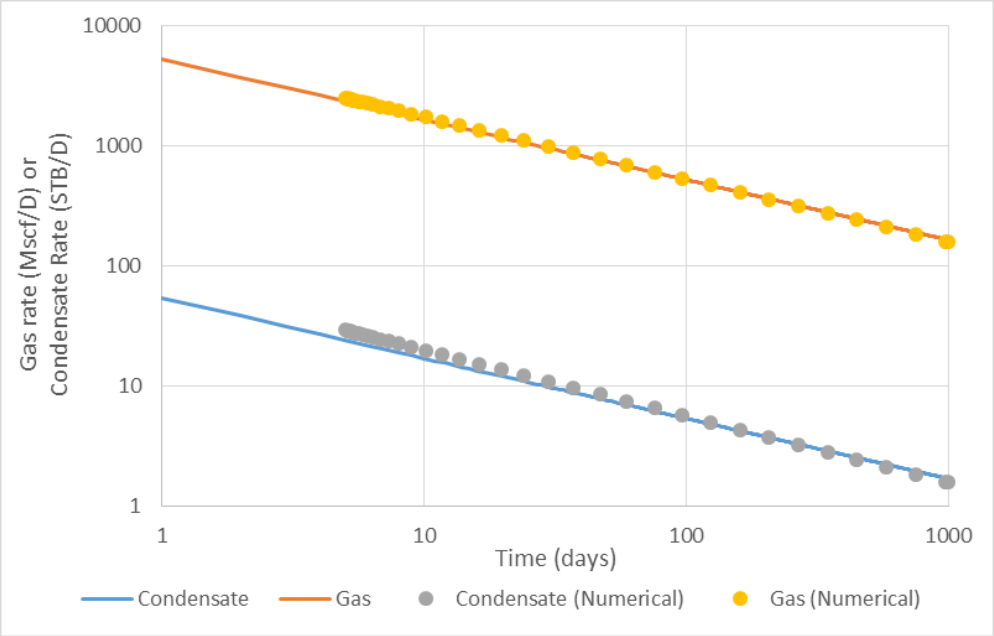

Figure 2.6. Log-log plot of condensate and gas rates for case 1.

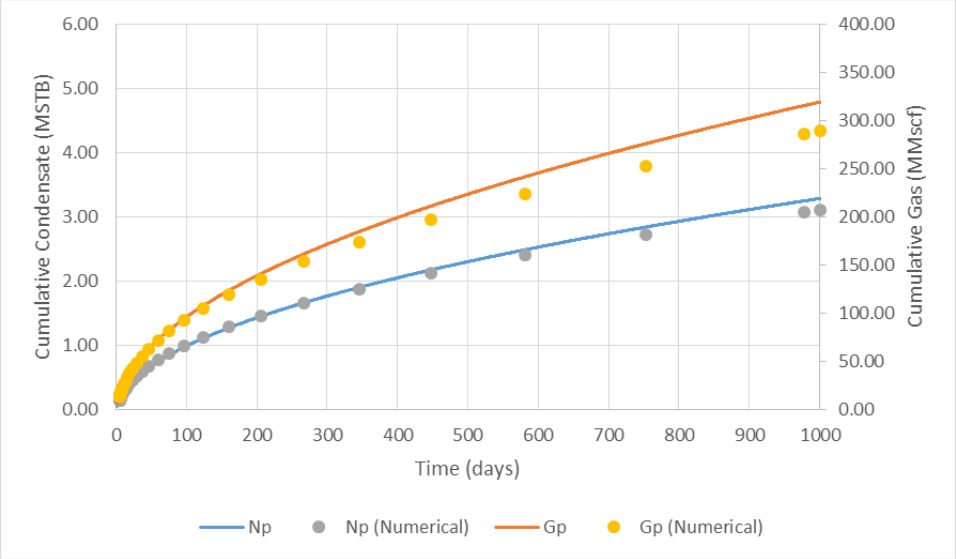

Figure 2.7. Cumulative condensate and gas production for case 1.

Shahamat et al. (2014) used the distance of investigation concept to the treat the flow as a "succession of pseudo-steady states," to calculate flowing pressures (at constant-rate condition) or flowing rates (at constant-flowing–pressure condition), but

focused on single phase gas or oil reservoirs. In the present work, transient flow is treated in similar fashion but extended to multi-phase flow of oil and gas. Further, variable operating conditions are accounted for rigorously. Later in this work, we use this method for production optimization, where the bottom-hole pressure might be changing at every control step in the optimal well control. Therefore, to use the analytical model in the optimization algorithm, this model should be valid for cases with varying bottom-hole pressure.

In this part, we investigate the effect of varying well-flowing pressure on the production rates. Case 2 has the same reservoir and fluid properties as case 1. In this case, we keep the BHP as 5000 psi for 250 days and then drop the pressure gradually to 1000 psi every 50 days from the 250th day to the 800th day, as shown in Figure 2.8. Figure 2.9 shows the average pressure in the investigated area at each time step. Figure 2.10 shows the corresponding gas and condensate production rates.

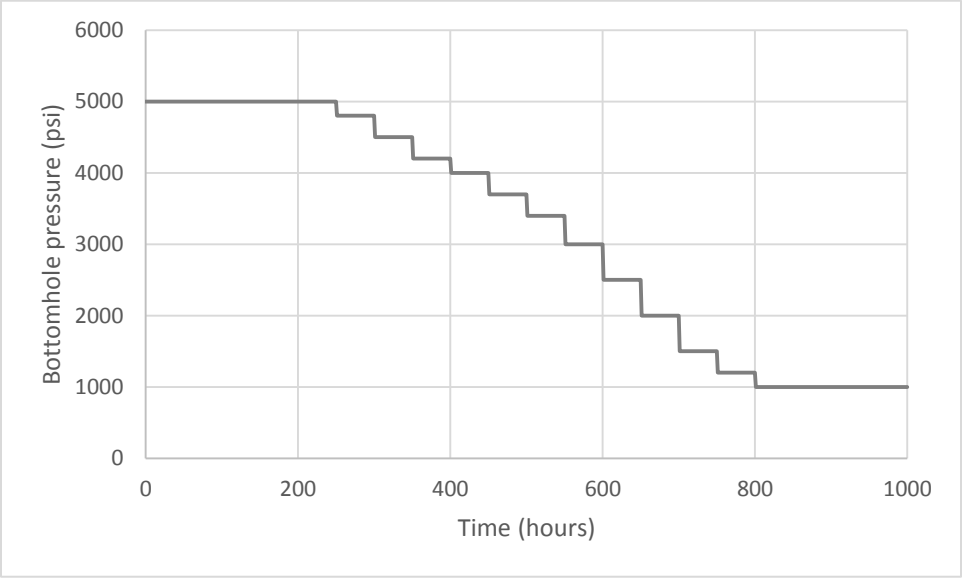

Figure 2.8. Bottom-hole pressure for case 2.

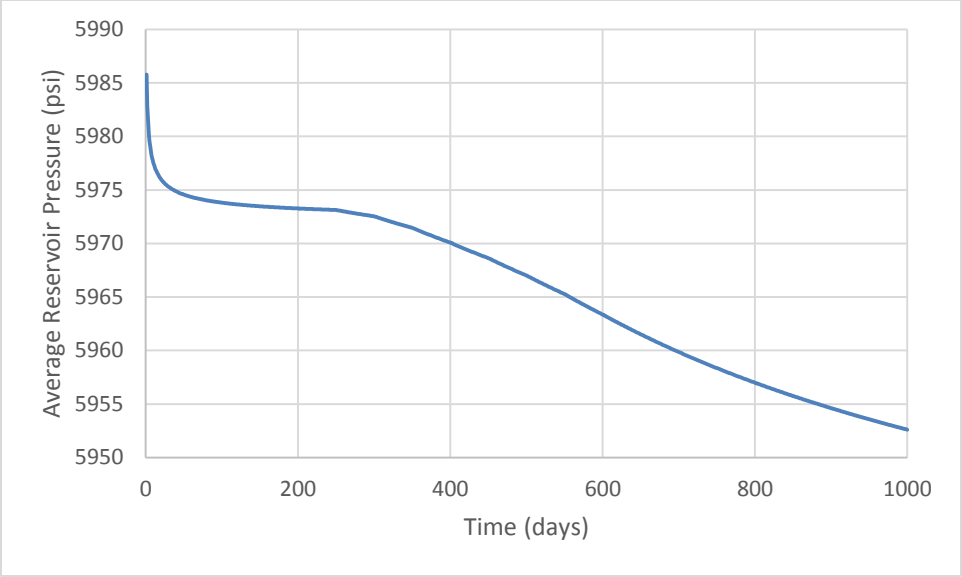

Figure 2.9. Average pressure in the investigated area for case 2.

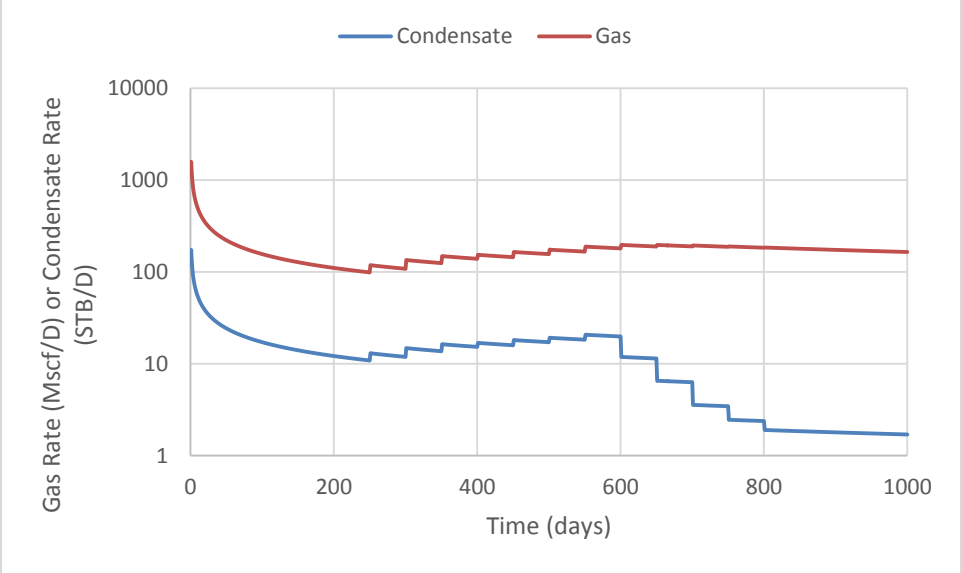

Figure 2.10. Semi-log plot of condensate and gas rates for case 2.

In this case, the gas and condensate production rates are decreasing in the first 250 days with the constant BHP pressure of 5000 psi. At the beginning of each pressure drop, there exists a spike on both production rates. Later as we keep the pressure to be

constant, production rates decrease again. But the overall production rates tend to increase as we decrease the pressure from 5000 psi to 3000 psi. However, when the BHP drops below the dew point at 3000 psi, the overall trend for gas production rates is decreasing from 600th to 800th day. At the same time, oil production rate tends to decrease much more. This is because the vaporized oil-gas ratio (R_v) as a function of pressure stays constant above the dew point but decreases with pressure when it is below the dew point. Figure 2.11 shows the cumulative production rate of both oil and gas.

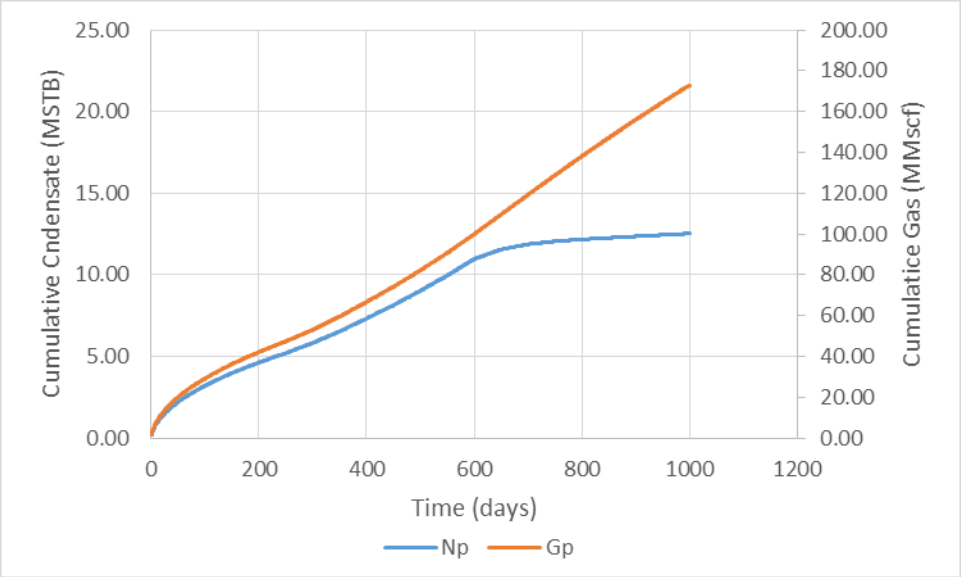

Figure 2.11. Cumulative gas and condensate production rates for case 2.

The final cumulative condensate from case 2 (12.52 MSTB) is almost four times of that from case 1 (3.11 MSTB). The final cumulative gas is about 60% of case 1. Since the condensate is much more expensive than gas, we can expect a much higher NPV with case 2. This demonstrates that different well schedules have important impact on the revenue. This will be discussed in detail in optimization part in chapter 4.

To see the forecasting performance of this analytical method during boundary dominated flow period, we increase the permeability from 0.05 md to 0.2 md. Here the pressure propagates to the boundary after 240 days. Figure 2.12 shows the average pressure in the investigated area p_{inv} during the simulation. As shown in figure 2.10, p_{inv} drops faster in the boundary dominated regime.

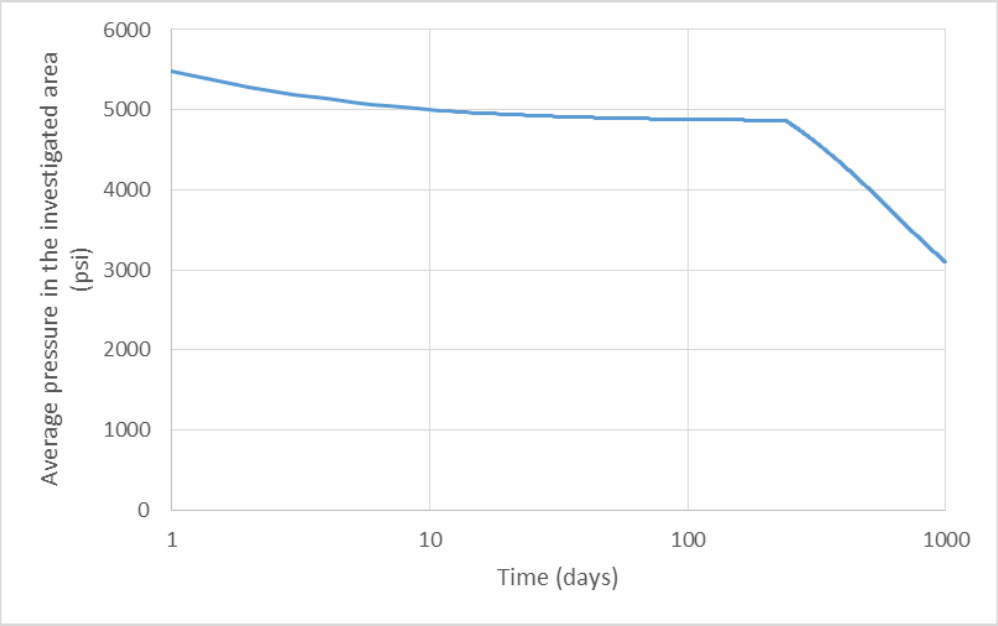

Figure 2.12. Average pressure in the investigated area for case 3.

Figure 2.13 represents the log-log plot of the gas and condensate production rates. Similar to case 1, both rates display half slope during the transient linear flow regime, while in boundary dominated flow both rates drop faster due to the greater pressure drop. The cumulative production of gas and condensate are shown in Figure 2.14.

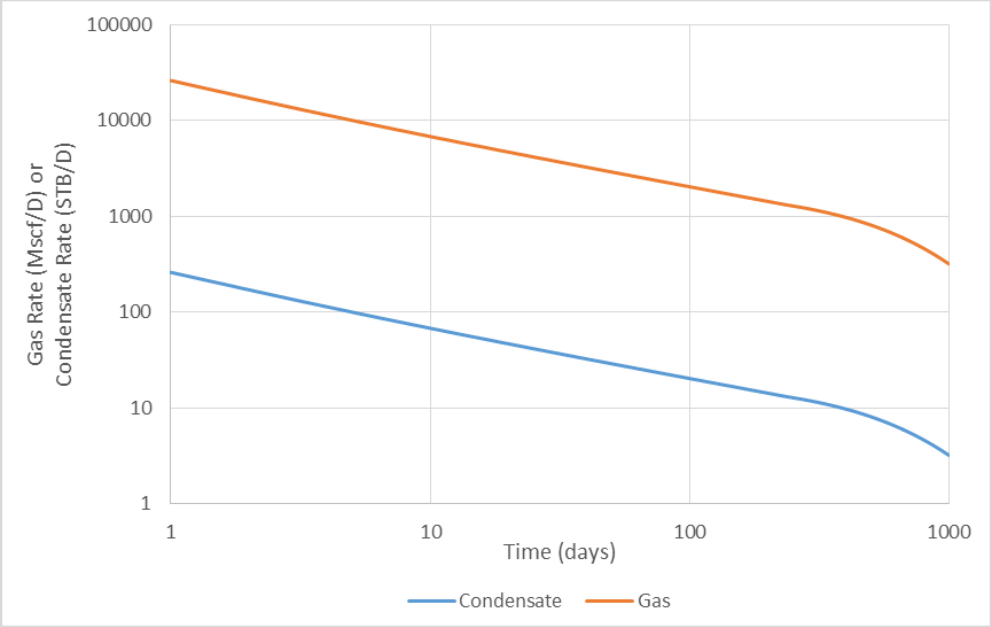

Figure 2.13. Log-log plot of condensate and gas rates for case 3.

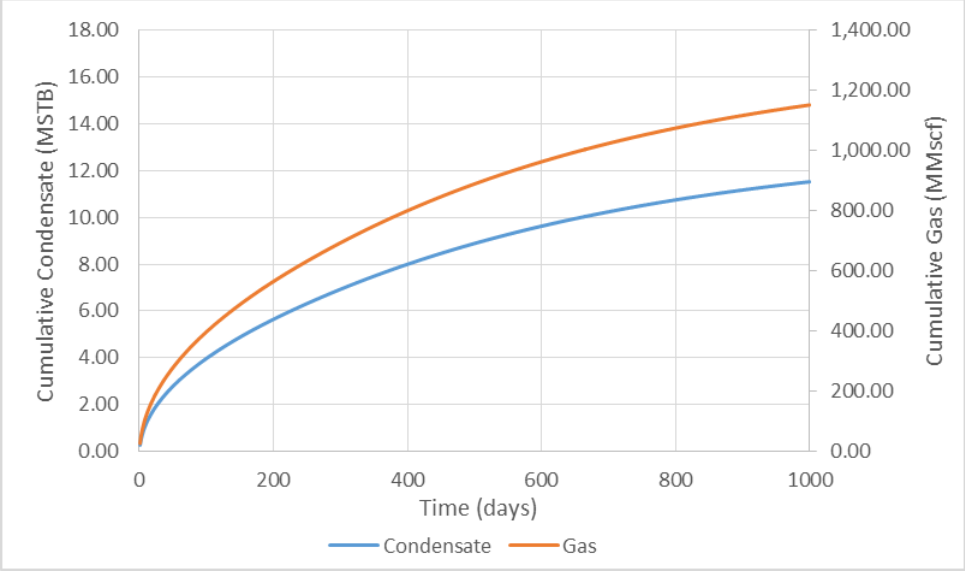

Figure 2.14. Cumulative condensate and gas production for case 3.

Case 4 is a two-phase oil case with constant flowing pressure of 1000 psi and static absolute permeability of 0.01 md. The reservoir size is 20000 ft × 200 ft × 50 ft. It is producing from a horizontal well intercepted by ten fractures with the total fracture

half- length of 1000 ft. Initially, it is a single phase oil reservoir ($S_{oi} = 1$) with the porosity of 0.1. The initial reservoir pressure is 6000 psi, and the bubble point pressure is 5000 psi. Reservoir temperature is 250 $°F$. The oil gravity is 40 $°API$ and the gas specific gravity is 0.65. Figures 2.15 and 2.16 show the PVT properties of oil and gas respectively and Figure. 2.17 corresponds to relative permeability curve.

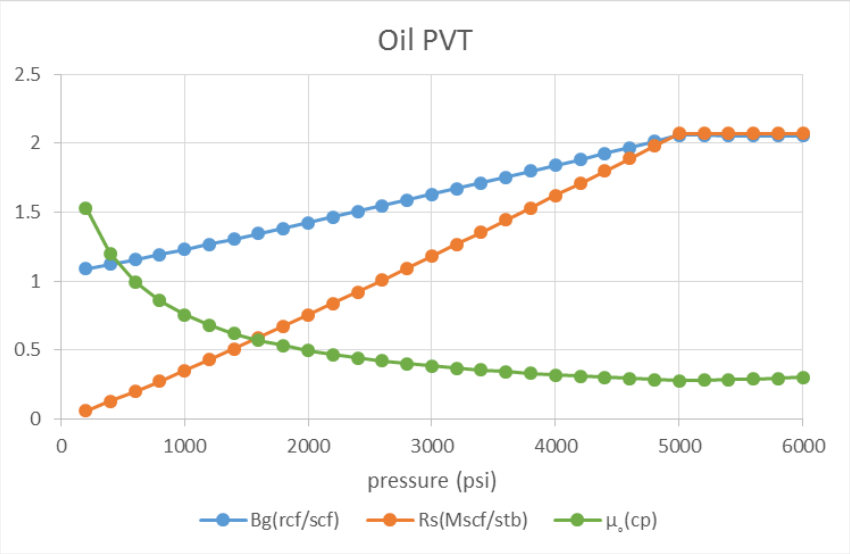

Figure 2.15. Oil PVT properties.

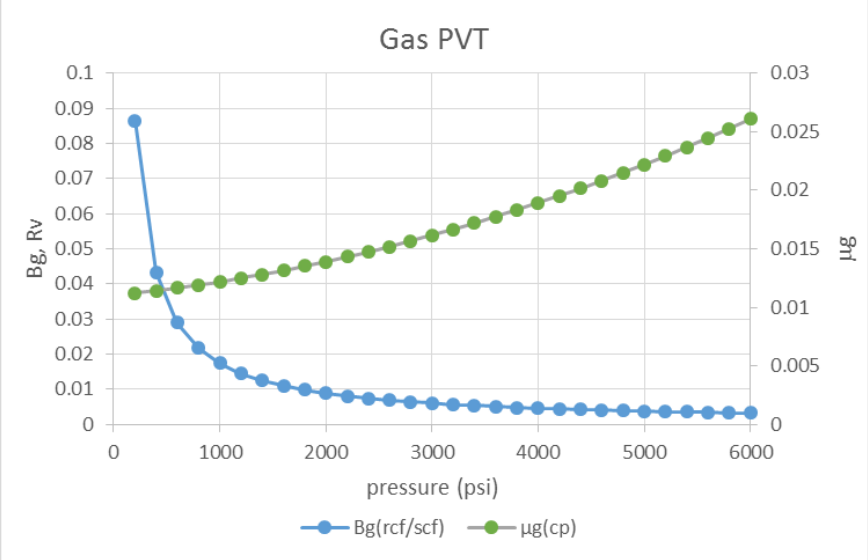

Figure 2.16. Gas PVT properties.

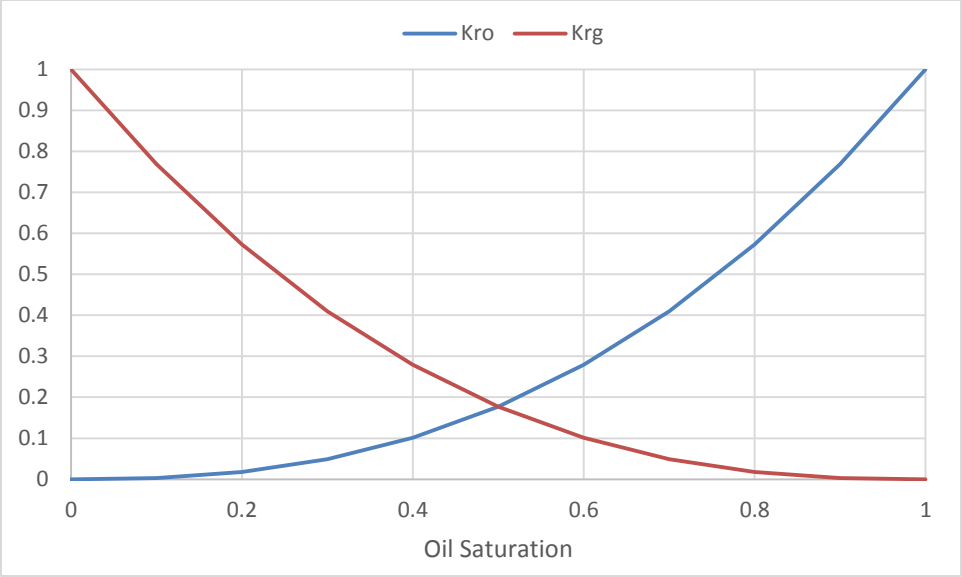

Figure 2.17. Relative permeability curves of oil and gas.

Figs. 2.18 and 2.19 represent the results from the analytical forecast methodology of a two phase oil case. As shown in Figure 2.18 both condensate and gas production rates have (-0.5) slope on a log-log plot. During the transient linear flow regime, the gas rate and condensate rate drop at the same rate, after we reach to the boundary, the oil rate starts to drop faster. The average pressure in the investigated area has a higher effect on oil recovery. However, even with a significant average pressure drop, the gas production rate does not change much.

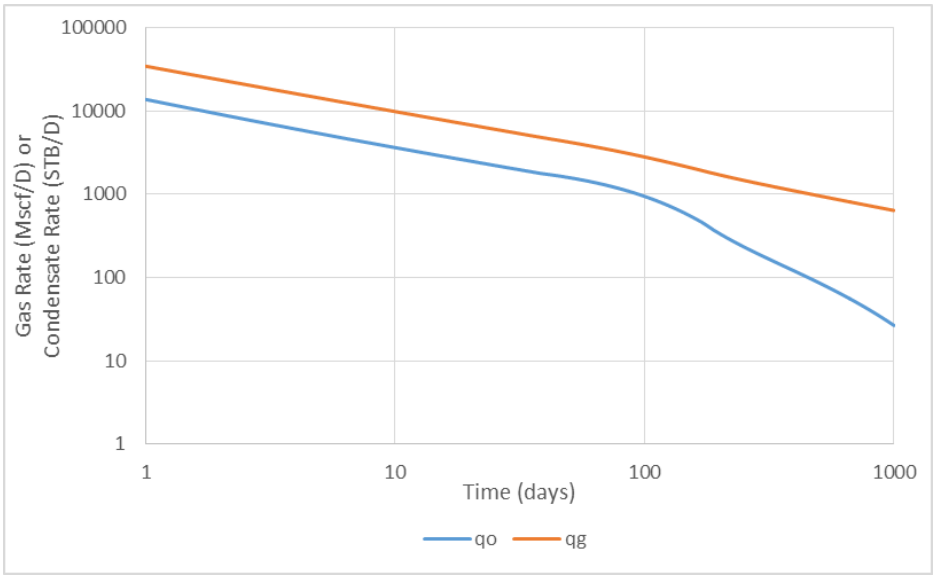

Figure 2.18. Log-log plot of condensate and gas rates for case 4.

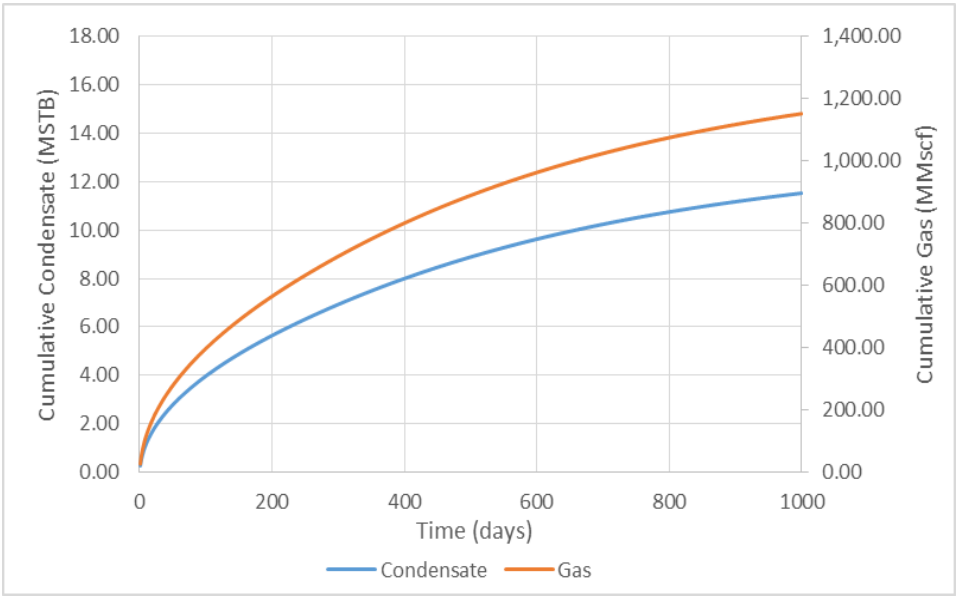

Figure 2.19. Cumulative condensate and gas production for case 4.

CHAPTER 3

HISTORY MATCHING

History matching is a process of determining plausible values of model parameters given uncertain measurements. Model parameters are the physical properties of the reservoir system, which usually contains permeability, porosity, relative permeability related parameters. In other words, history matching is an assumed theoretical model which relates the observed data to the model variables, where a plausible solution must be consistent with the observed data and physical constraints. The theoretical model characterizes an approximation to the real physical relation between physical, geometric properties and data.

In this study, following by Oliver et al. (2008), the history matching problem is assumed to be the same as minimizing an objective function. The objective function consists of the sum of a data mismatch term and regularization term which is normally based on a prior geostatistical model. The objective function is defined by

$$O_j(m) = \frac{1}{2}\left(d_{uc,j} - g(m)\right)^T C_D^{-1}\left(d_{uc,j} - g(m)\right) + \frac{1}{2}\left(m - m_{uc,j}\right)^T C_M^{-1}\left(m - m_{uc,j}\right), \tag{3.1}$$

where m is the vector of model parameters, C_D is the matrix of measurement errors, C_M is the prior covariance matrix of model parameters, $m_{uc,j}$ is a sample from $N(m_{pr}, C_M)$, $d_{uc,j}$ is a vector of perturbed observations sampled from $N(d_{obs}, C_D)$ and $g(m)$ is the data predicted from the reservoir simulator. Here, m_{pr} is the prior mean of the model and

d_{obs} is the vector of observed data.

One way to minimize the objective function $O_j(m)$, given in Eq. (3.1), is to implement the ensemble smoother with multiple data assimilations (ES-MDA) proposed by Emrick and Reynolds (2013) to improve the ensemble Kalman filter (EnKF) (Evensen, 1994) which obtains a better data match and provides a better quantification of uncertainty. Because EnKF updates both model parameter and states at each assimilation step, which often yields to a relatively poor data match. With EnKF, there exists potential inconsistency between the updated model parameters and states for problems where the relation between the reservoir model parameters and data predicted from the reservoir simulator is highly nonlinear. Unlike EnKF that assimilates data sequentially, the ensemble smoother (ES) assimilate all data available simultaneously and update only reservoir model parameters. ES-MDA was introduced by the analogy between the ensemble smoother and one Gauss-Newton correction. Using the same update method for the ES, this method assimilates the same set of data N_a times with an inflated covariance matrix of the measurement errors, which is to say, at the l^{th} data assimilation step, the measurement covariance matrix C_D is multiplied by inflation factor $\alpha_l > 1$. Simply put, the algorithm of ES-MDA method is given as follows:

Algorithm 1 Pseudo-code for ES-MDA

Choose the number of data assimilations $\boldsymbol{N_a}$and the inflation coefficients of the data covariance matrix $\boldsymbol{\alpha_l}$.

For $\boldsymbol{l = 1}$ to $\boldsymbol{N_a}$

1. Run the ensemble from $\boldsymbol{t = o}$.
2. For each ensemble member, perturb the observation vector using

$$\boldsymbol{d_{uc,j} = d_{obs} + \sqrt{\alpha_l} C_D^{1/2} Z_j}.$$

3. Update the ensemble member, $\boldsymbol{j}$, using

$$\boldsymbol{m_j^a = m_j^f + C_{MD}^f \left(C_{DD}^f + \alpha C_D \right)^{-1} \left(d_{uc,j} - d_j^f \right)}.$$

End For

In the above algorithm, C_{MD} is the cross-covariance matrix between the vector of the model parameter and the vector of predicted data, defined as

$$C_{MD} = \frac{1}{N_e - 1} \sum_{j=1}^{N_e} \left(m_j^f - \bar{m}^f \right) \left(d_j^f - \bar{d}^f \right)^T,$$

where

$$\bar{m}^f = \frac{1}{N_e} \sum_{j=1}^{N_e} m_j^f$$

and

$$\bar{d}^f = \frac{1}{N_e} \sum_{j=1}^{N_e} d_j^f.$$

C_{DD} is the auto-covariance matrix of predicted data given by:

$$C_{DD} = \frac{1}{N_e - 1} \sum_{j=1}^{N_e} \left(d_j^f - \bar{d}^f \right) \left(d_j^f - \bar{d}^f \right)^T.$$

As an example, we implement the ES-MDA method on case 1 in chapter 2. This case is a gas condensate reservoir with a constant flowing pressure of 1000 psi and static absolute permeability of 0.005 md. The reservoir size is 20000 ft × 200 ft × 50 ft. It is producing from a horizontal well intercepted by ten fractures with the total fracture half-length of 1000 ft. Initially it is a single phase gas reservoir ($S_{oi} = 0$) with the porosity of 0.08. The initial reservoir pressure is 6000 psi, and the dew point pressure is 3000 psi. Reservoir temperature is 250 °F. The production history of oil and gas is matched to get a true description of the PVT data.

Figure 3.1 and 3.2 show the q_o and q_g from the prior ensemble. Figure 3.3 and 3.4 show the q_o and q_g from the final posterior ensemble. Red line is the true model and grey lines denote the ensemble member results. The results show that after four time data assimilation, the parameters are matched and uncertainties are decreased as well.

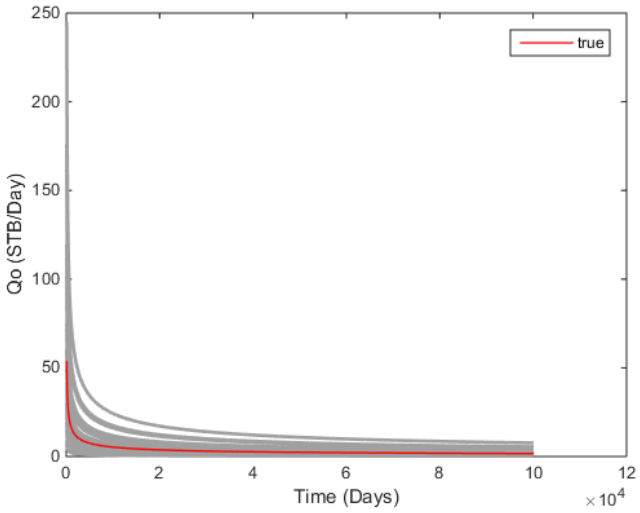

Figure 3.1. q_o from the prior ensemble.

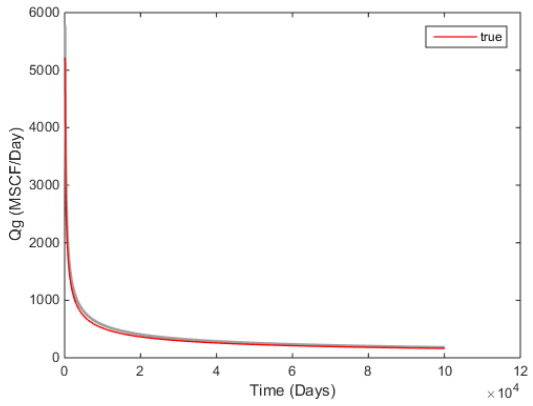

Figure 3.2. q_g from the prior ensemble.

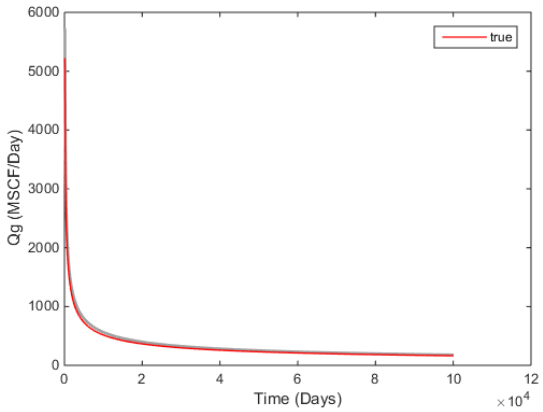

Figure 3.3. q_o from the final posterior ensemble.

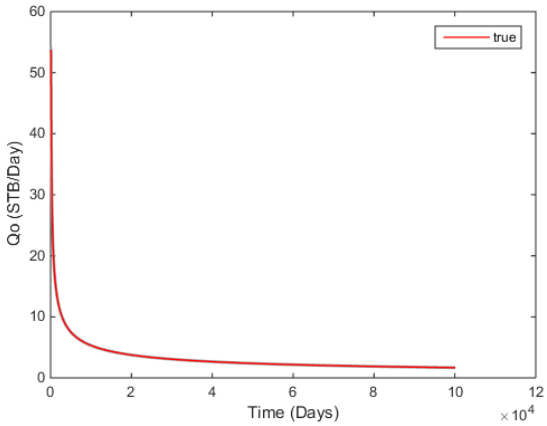

Figure 3.4. q_g from the final posterior ensemble.

CHAPTER 4

OPTIMIZATION

The ultimate goal of reservoir development is to achieve the optimum profitability from the well or field. Once a true reservoir description is available, well control optimization is implemented to carry out the optimal well control which leads to maximum net present value.

4.1 Optimization Algorithm

In this work, a line search steepest descent method combined with the simplex gradient is carried out for well control optimization. The objective function is

$$\max_x f(x) = NPV, \tag{4.1}$$

where vector $\boldsymbol{x}$ denotes the well control. And the calculation of net present value is given by

$$NPV = \sum_{n=1}^{N_t} \frac{r_o^n q_o^n - r_w^n q_g^n}{1+b^{t_n/_{365}}}, \tag{4.2}$$

where N_t is the number of time steps; r_o^n and r_w^n denote oil/gas revenue over time step n, respectively; q_o^n and q_g^n are the average oil/gas production rates over the n^{th} time step; b is the annual discount rate.

Starting from the initial guess of the well control as a vector x, we used the line search steepest-descent method to update well control. The line search method follows:

1. Choose a direction p_k,

2. Search along this direction from x_k to find a new iterate x_{k+1} with a lower/higher function value,
3. The distance to move along p_k can be found by solving a 1-D minimization problem.
4. New iterate is updated by

$$x_{k+1} = x_k + \alpha_k p_k. \tag{4.3}$$

In practice, we write the scheme as,

$$x_{k+1} = x_k + \alpha_k \frac{p_k}{\|p\|_\infty}, \tag{4.4}$$

In each iteration, we need to compute a search direction p_k, and decide how far to move along this direction, or determine the stepsize α_k. Line search algorithm tries out a sequence of candidate values for α_k, stopping to accept one of those values when certain conditions is satisfied, e.g. the value of the objective is sufficiently decreased. The approximation of α should satisfy either first wolf condition or second wolf condition, or the Goldstein condition. The backtracking algorithm is applied to find α_k. Once the search direction is determined, it searches for an initial α_k^0 to update the new iteration. If the new update returns a higher objective function value, then accept this stepsize and complete the optimization iteration. Otherwise, cut the step sized by half and repeat.

The stochastic simplex approximate gradient (StoSAG), is used in this work to approximate the gradient. The gradient is calculated by:

$$\nabla \hat{f} = \Delta \hat{X}^{-T} \Delta \hat{F}^T, \tag{4.5}$$

where $\Delta \hat{X}^{-T}$ is the pseudoinverse of $\Delta \hat{X}^T$ obtained by single value decomposition. The calculation of $\Delta \hat{X}$ is

$$\Delta \hat{X} = [\delta \hat{x}^1, \delta \hat{x}^2, \delta \hat{x}^3, \dots, \delta x^{Ne}] = [\hat{x}^1 - \bar{x}, \hat{x}^2 - \bar{x}, \dots, \hat{x}^{Ne} - \bar{x}], \tag{4.6}$$

where N_e is the ensemble size; $\bar{x}$ is the sample mean of $\hat{x}^j$,

$$\bar{x} = \frac{1}{N_e}\sum_{j=1}^{Ne} \hat{x}^j, \tag{4.7}$$

where $\hat{x}^j$ is the j^{th} perturbation of x_k. The following procedures explains how to sample $\hat{x}^j$ at each iteration:

1. at iteration k, we assume $x \sim N(x_k, C_x)$;
2. decompose C_x using cholesky decomposition, i.e. $C_x = LL^T$;
3. sample Z^j from $N(0, I)$;
4. $\hat{x}^j = x_k + LZ^j$.

And $\Delta\hat{F}$ is calculated by

$$\Delta\hat{F} = \left[\delta\hat{f}^1, \delta\hat{f}^2, \delta\hat{f}^3, \dots, \delta\hat{f}^{Ne}\right] = [\hat{f}^1 - \bar{f}, \hat{f}^2 - \bar{f}, \dots, \hat{f}^{Ne} - \bar{f}], \tag{4.8}$$

$\hat{f}^j$ is the function value corresponding to $\hat{x}^j$; $\bar{f}$ is the defined by

$$\bar{f} = \frac{1}{N_e}\sum_{j=1}^{Ne} \hat{f}^j = \frac{1}{N_e}\sum_{j=1}^{Ne} f(\hat{x}^j). \tag{4.9}$$

In summary, the optimization iterations follow the steepest ascent scheme combined with the backtracking line search, shown in Algorithm 2. The convergence criteria are set to be either

$$\tau_x^* = \frac{|f(x_{k+1}) - f(x_k)|}{\max\{|f(x_k)|, 1.0\}} \leq 10^{-4} \tag{4.10}$$

or

$$\tau_f^* = \frac{||x_{k+1} - x_k||_2}{\max\{||x_k||_2, 1.0\}} \leq 10^{-3}. \tag{4.11}$$

The algorithm will stop when maximum number of simulations is reached, or consecutive failures in improving the NPV within a specified number of iterations are reached.

Algorithm 2 Pseudo-code for steepest ascent using StoSAG

Initialize the parameters including the maximum step size $\boldsymbol{\alpha_0}$, the maximum allowed number of step size cuts $\boldsymbol{n_{sc}}$, the maximum number of the consecutive search direction re-computation $\boldsymbol{n_{ss}}$, the maximum allowed simulation number $\boldsymbol{n_s}$, and the number if perturbation samples $\boldsymbol{N_p}$. Set the number of simulation $\boldsymbol{n_{sim} = 0}$, the number of step size cuts $\boldsymbol{n_{cuts} = 0}$, the number of search direction re-computation is 0, the step size as $\boldsymbol{\alpha_k = \alpha_0}$.

Do While ($\boldsymbol{n_{sim} \leq n_s}$)

4. Compute the search direction using Eq. (4.5). Set $\boldsymbol{is = is + 1}$.
5. Compute a trial update $\boldsymbol{x_{k+1}^{trial} = x_k + \alpha_k \times p_k}$.
6. Check is the trial update is acceptable:
   - If $(\boldsymbol{f(x_{k+1}) > f(x_k)})$ then

     $\boldsymbol{x_{k+1} = x_{k+1}^{trial}}$, $\boldsymbol{k = k + 1}$, $\boldsymbol{is = 0}$, $\boldsymbol{n_{cuts} = 0}$, $\boldsymbol{\alpha_k = \alpha_0}$.
   - Else

     If $\boldsymbol{n_{cuts} > n_{sc}}$ and $\boldsymbol{is > n_{ss}}$, terminate,

     If $\boldsymbol{n_{cuts} > n_{sc}}$ and $\boldsymbol{is < n_{ss}}$, then go to step 1,

     If $\boldsymbol{n_{cuts} \leq n_{sc}}$ set $\boldsymbol{\alpha_k = \alpha_k/2}$, then go to step 2.
   - End if
7. Terminate if convergence criteria is satisfied.

End Do

4.2 Optimization Solution

Recalling chapter 2, a different well schedule can result in very different final net present value of a same reservoir. In this section, we implement the optimization algorithm to explore the potential of the reservoir. Here, the oil price is 50 $/STB, the gas price is 1.5 $/Mscf, and the inflation rate 0.1. One key character of condensate gas reservoirs is the vaporized oil ratio. The goal is to produce more condensate on the surface, which results in higher revenue. Generally in a single phase flow reservoir, we

obtain the maximum production rate at the lowest possible BHP. However in a multiphase flow condensate gas reservoir, as we drop the BHP, the R_v value decreases, result in less condensate production on the surface. In order to maximize the condensate production, we are looking for an optimal well schedule leading to maximum revenue.

To investigate the effect of vaporized oil gas ratio on the optimal well control, we consider five cases with different R_v curves. For all cases, the reservoir and fluid properties other than R_v are the same as the case 1 in chapter 2. The initial guess for the well schedule is shown in Figure 4.1. Figure 4.2 shows the R_v as a function of pressure for these cases.

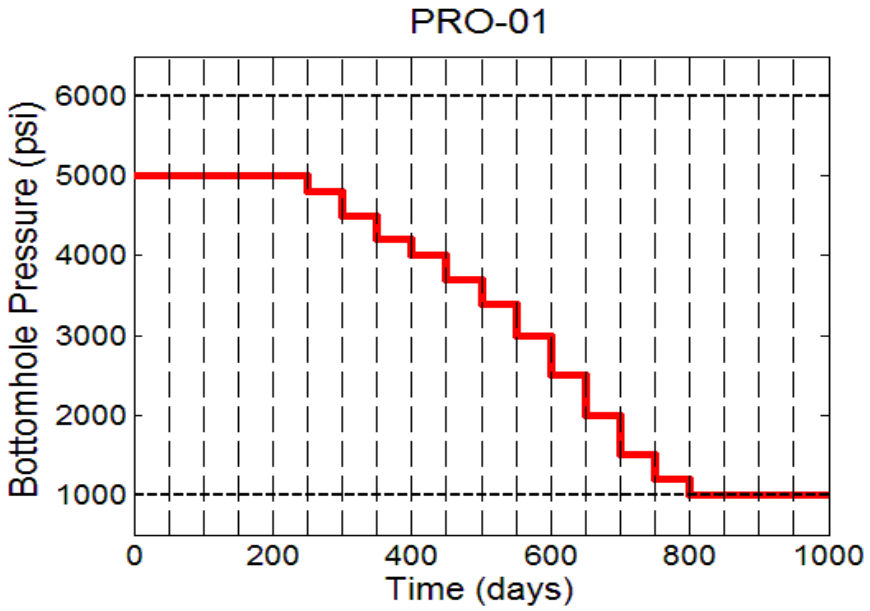

Figure 4.1. Initial well schedule

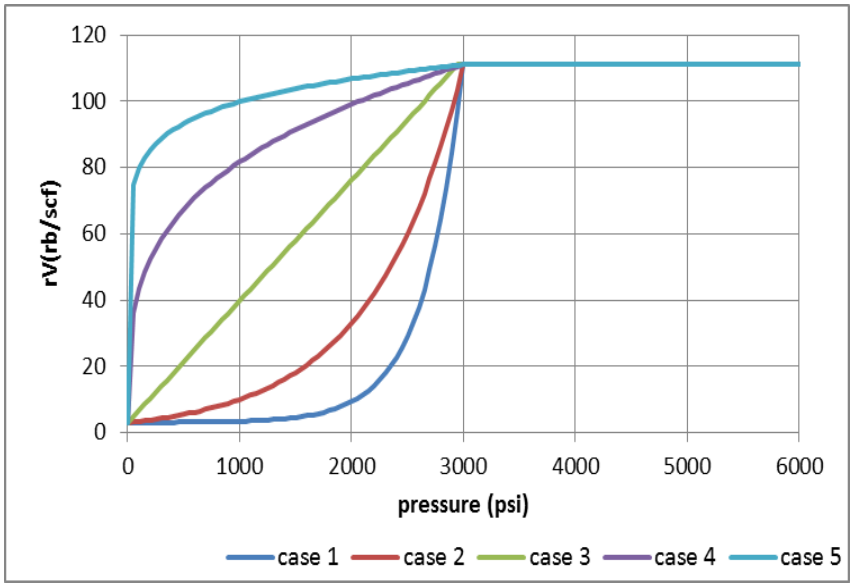

Figure 4.2. R_v vs. pressure.

4.2.1 Case 1

In case 1, we use the corresponding R_v curve shown in dark blue in Figure 4.2. Figure 4.11 shows the increase of NPV with respect to simulation numbers. As observed, the optimization curve is composed of two parts: a steeper part and a flatter part. The NPV obtained by the initial well setting is 0.074582 million dollars. Totally after 11 iterations (339 simulations), the final NPV is 0.84608 million dollars, which is about 11.34 times as much as the initial NPV. The total increase of NPV is 0.7715 million dollars. The increase of NPV in the steeper part is 0.753 million dollars, contributing 97.6% of the total increase in 2 iterations (24 simulations). The increase of NPV in the flatter part is 0.0185 million dollars, which contributes 2.4% of the total increase in the other 9 iterations (315 simulations). Figure 4.4 shows the comparison of cumulative gas between initial well control and optimal well control. The final cumulative gas corresponding to the initial guess is 182 MMscf. After optimization, the final cumulative

gas is 289.23 MMscf, which is about 158.9% of the final cumulative gas obtained with the initial well control.

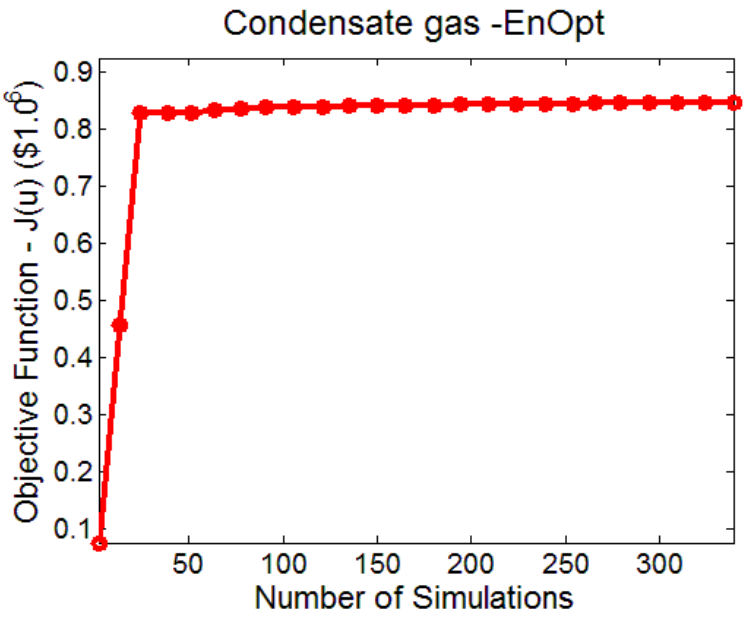

Figure 4.3. NPV vs. Numbers of simulations for case 1.

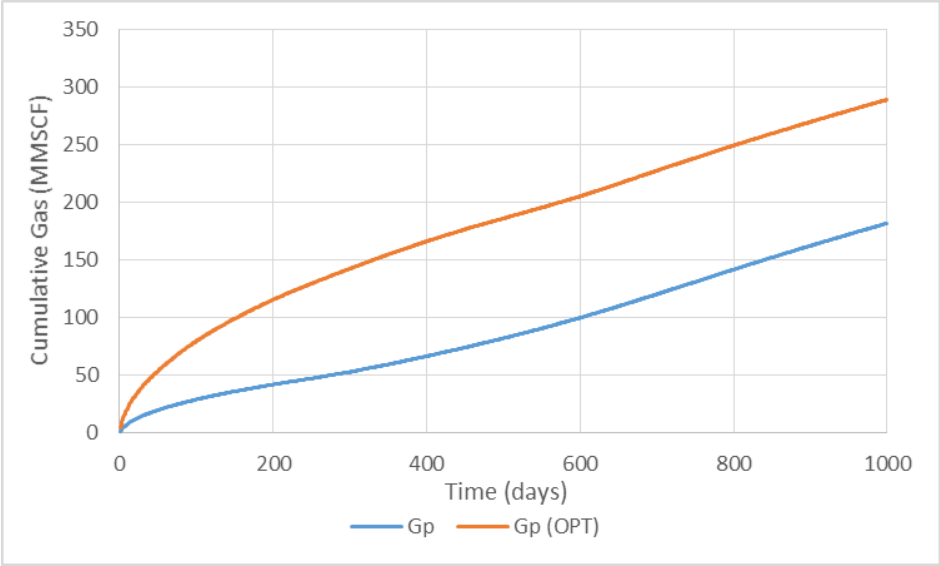

Figure 4.4. Cumulative gas comparison for case 1.

Figure 4.5 shows the comparison of cumulative condensate between initial well control and optimal well control. The final cumulative gas corresponding to the initial guess is 18.37 MSTB. The final cumulative condensate obtained with the optimal well control is 29.8 MSTB, which is about 162% of the final cumulative condensate obtained with the initial well control.

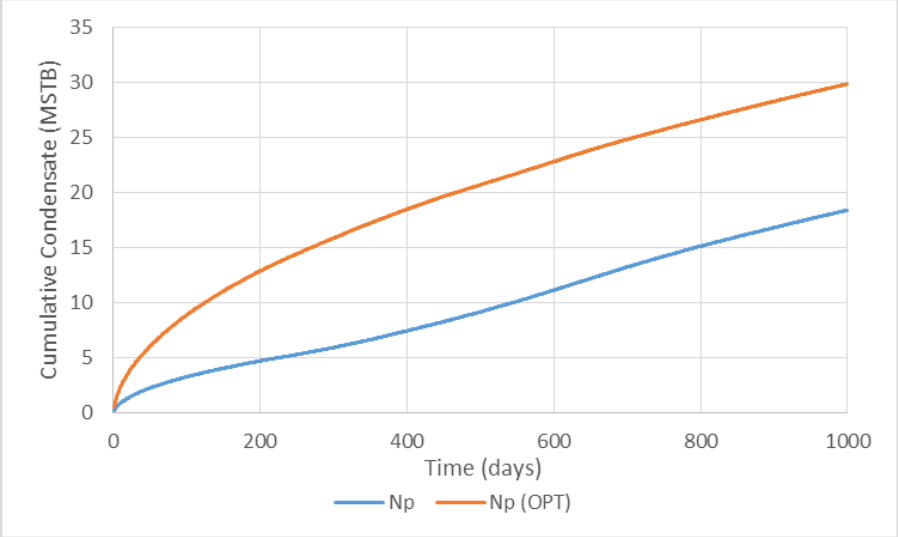

Figure 4.5. Cumulative condensate comparison for case 1.

Figure 4.6 shows the optimal well control. At the first 550 days the BHP stays around 3000 psi, which is the dew point pressure, and then it drops gradually to 1000 psi within 150 days. The small variation around 3000 psi during this period is due to the stochastic characters of the Simplex method. Since we are using the approximate gradient, it is difficult to find the real optimal solution. However, an approximate solution is still good enough.

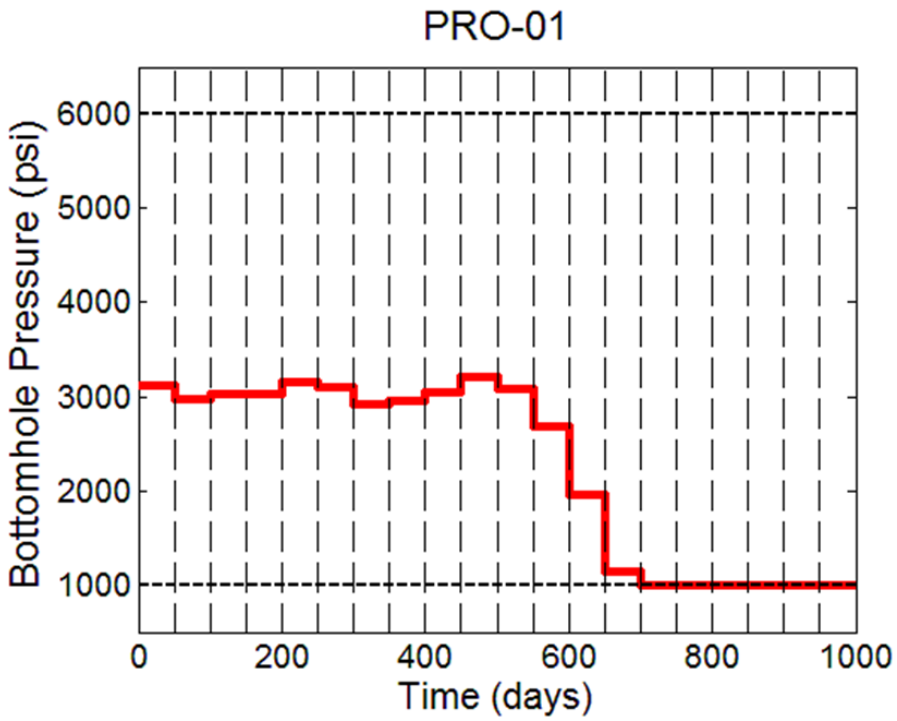

Figure 4.6. Optimal well control for case 1.

4.2.2 Case 2

In case 2, we use the corresponding R_v curve shown in red in Figure 4.2. Figure 4.7 shows the increase of NPV with respect to simulation numbers. The NPV obtained by the initial well setting is 0.16165 million dollars. Totally after 11 iterations (244 simulations), the final NPV is 0.97509 million dollars, which is about 6 times as much as the initial NPV. The total increase of NPV is 0.81344 million dollars. Figure 4.8 shows the comparison of cumulative gas between initial well control and optimal well control. After optimization, the final cumulative gas is 292 MMscf, which is about 165% of the final cumulative gas obtained with the initial well control (176.6 MMscf).

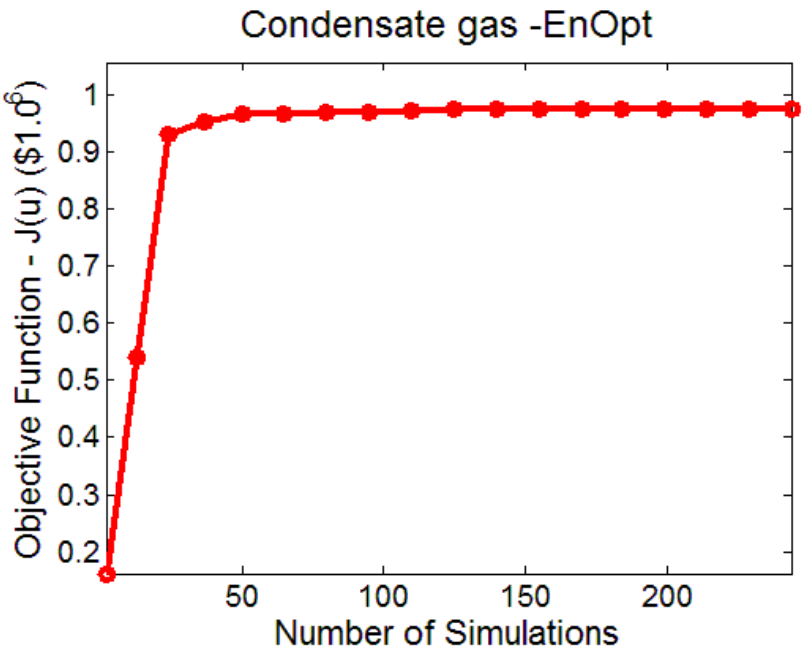

Figure 4.7. NPV vs. Numbers of simulations for case 2.

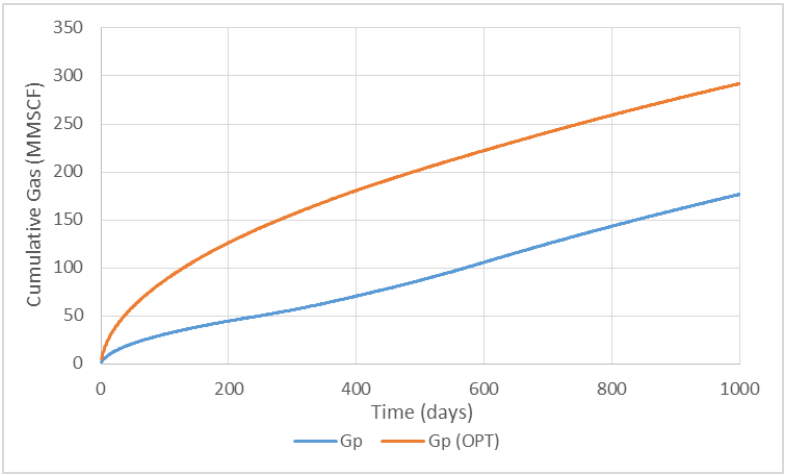

Figure 4.8. Cumulative gas comparison for case 2.

Figure 4.9 shows the comparison of cumulative condensate between initial well control and optimal well control. The final cumulative condensate obtained with the optimal well control is 43.73 MSTB, which is about 190% of the final cumulative condensate obtained with the initial well control (22.99 MSTB).

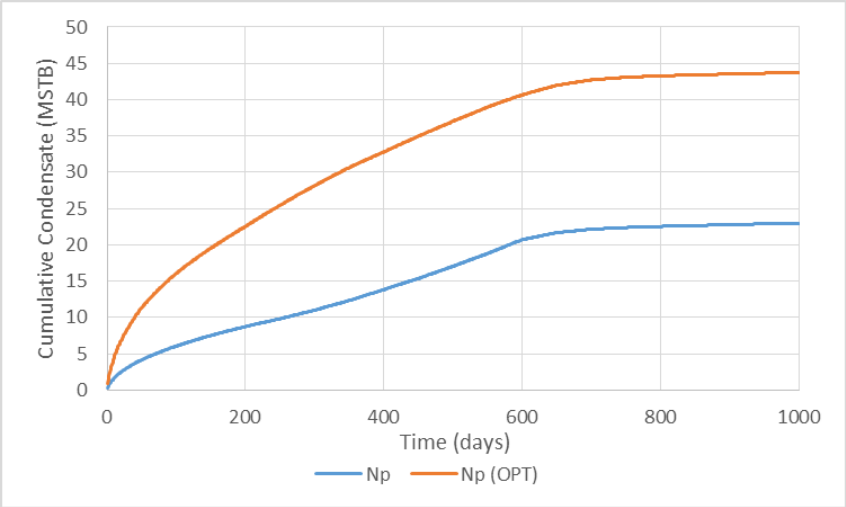

Figure 4.9. Cumulative condensate comparison for case 2.

Figure 4.10 shows the optimal well control. At the first 600 days the BHP stays around 3000 psi, which is the dew point pressure. Then it drops gradually to 1000 psi within 250 days. The pressure drop is slower compared with case 1. As shown in Figure 4.2, as pressure decreases, the R_v curve of case 1 has a sharper drop below the dew point compared with case 2, and stays almost constant below 2000 psi. However, in case 2, the R_v value decreases with pressure all the way down. Therefore, in case 2, the optimal BHP does not drop as fast as the one in case 1.

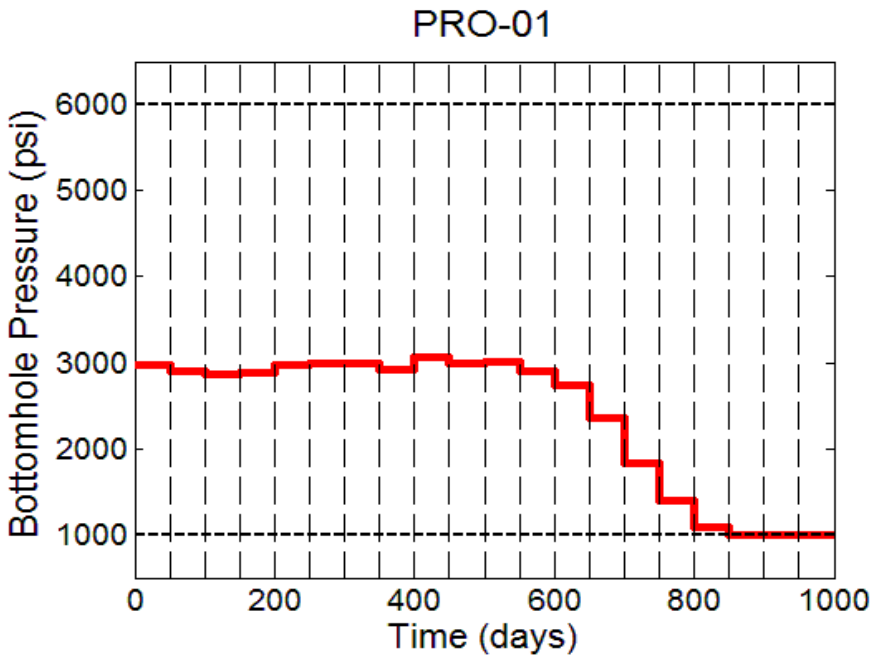

Figure 4.10. Optimal well control for case 2.

4.2.3 Case 3

In case 3, we use the corresponding R_v curve shown in green in Figure 4.2. Figure 4.11 shows the increase of NPV with respect to simulation numbers. The NPV obtained by the initial well setting is 0.93809 million dollars. Totally after 9 iterations (204 simulations), the final NPV is 1.7672 million dollars, which is about 1.89 times as much as the initial NPV. The total increase of NPV is 0.82911 million dollars. Figure 4.12 shows the comparison of cumulative gas between initial well control and optimal well control. After optimization, the final cumulative gas is 283.5 MMscf, which is about 59% higher than the final cumulative gas obtained with the initial well control.

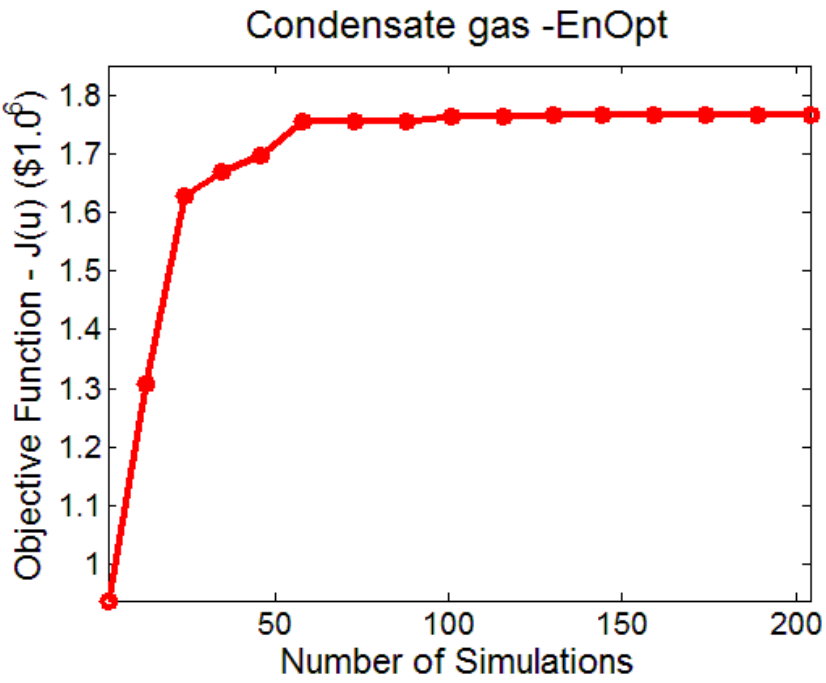

Figure 4.11. NPV vs. Numbers of simulations for case 3.

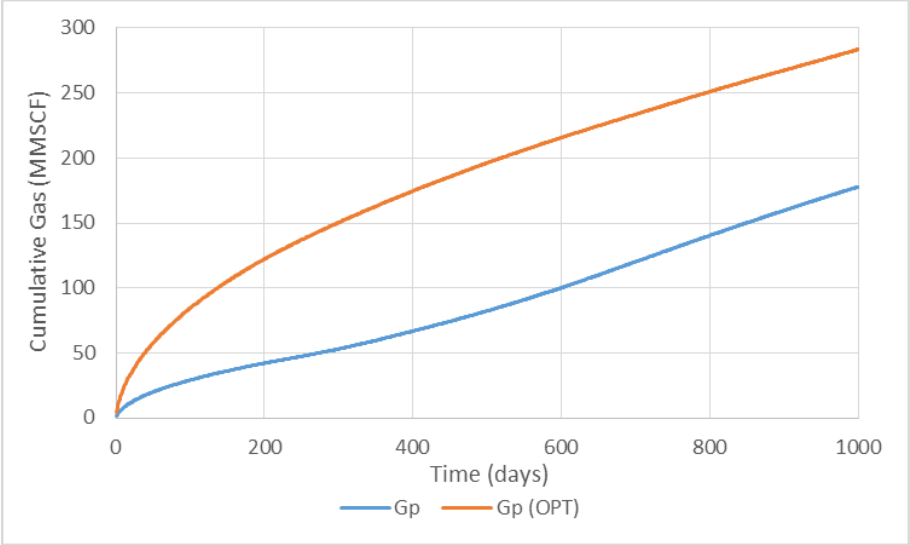

Figure 4.12. Cumulative gas comparison for case 3.

Figure 4.13 shows the comparison of cumulative condensate between initial well control and optimal well control. The final cumulative condensate obtained with the

optimal well control is 29.97 MSTB, which is about 93% higher than the final cumulative condensate obtained with the initial well control.

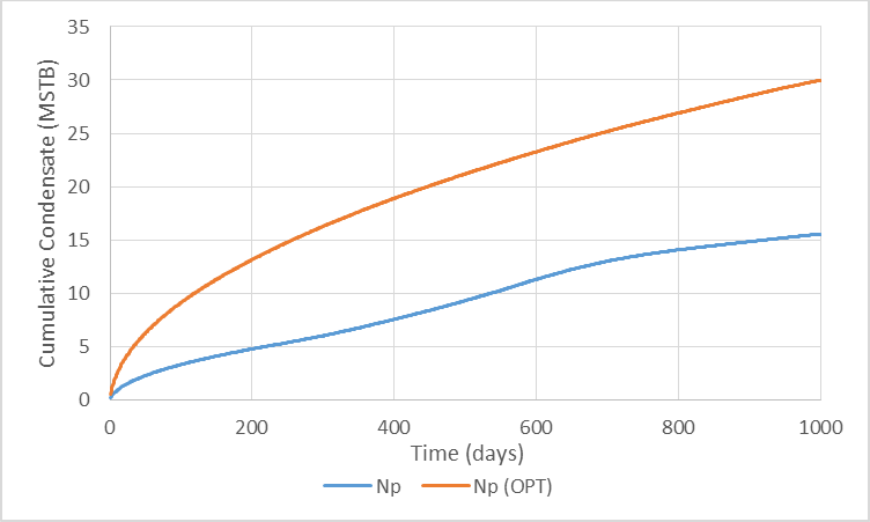

Figure 4.13. Cumulative condensate comparison for case 3.

Figure 4.14 shows the optimal well control for case 3. The BHP holds at around 2800 psi (slightly below the dew point).

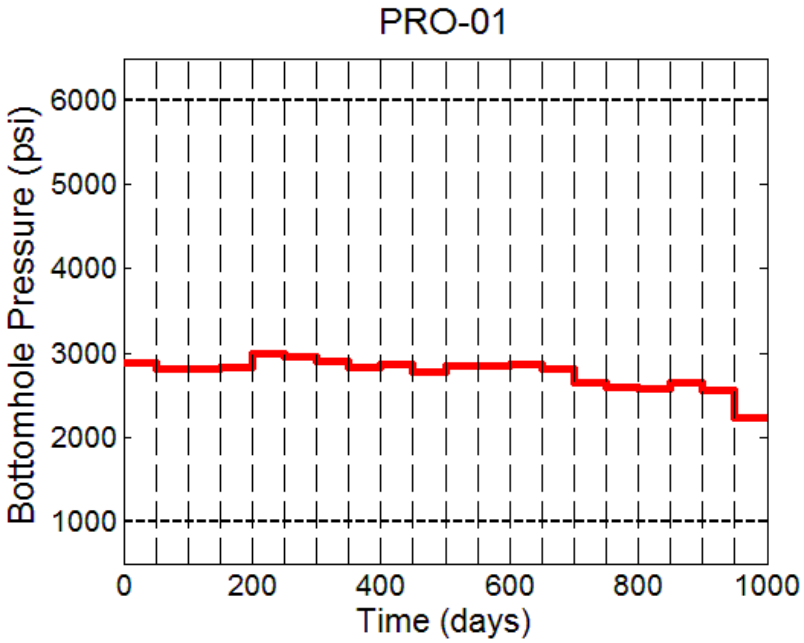

Figure 4.14. Optimal well control for case 3.

4.2.4 Case 4

In case 4, we use the corresponding R_v curve shown in purple in Figure 4.2. Figure 4.15 shows the increase of NPV with respect to simulation numbers. The NPV obtained by the initial well setting is 0.58737 million dollars. Totally after 8 iterations (154 simulations), the final NPV is 1.8999 million dollars, which is about 3.23 times as much as the initial NPV. The total increase of NPV is 1.3125 million dollars. Figure 4.16 shows the comparison of cumulative gas between initial well control and optimal well control. The final cumulative gas corresponding to the initial guess is 169.098 MMscf. After optimization, the final cumulative gas is 361.01 MMscf, which is about 213.5% of the final cumulative gas obtained with the initial well control.

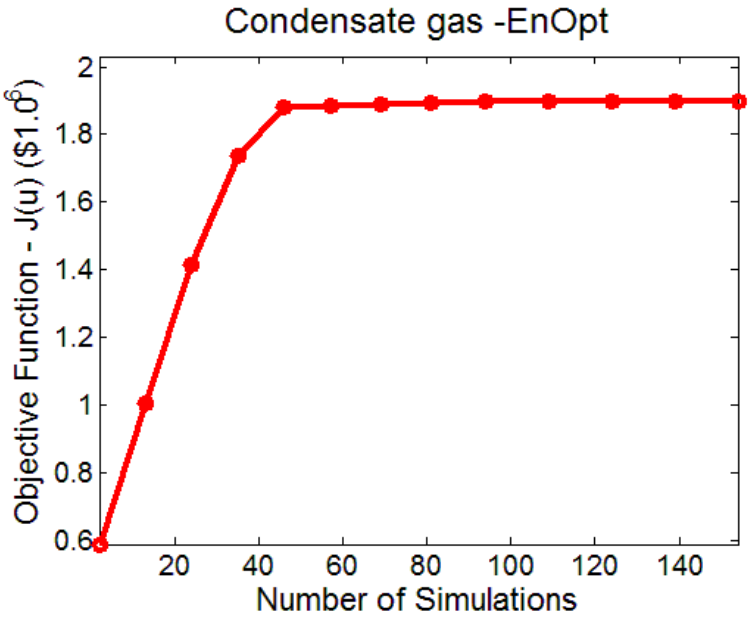

Figure 4.15. NPV vs. Numbers of simulations for case 4.

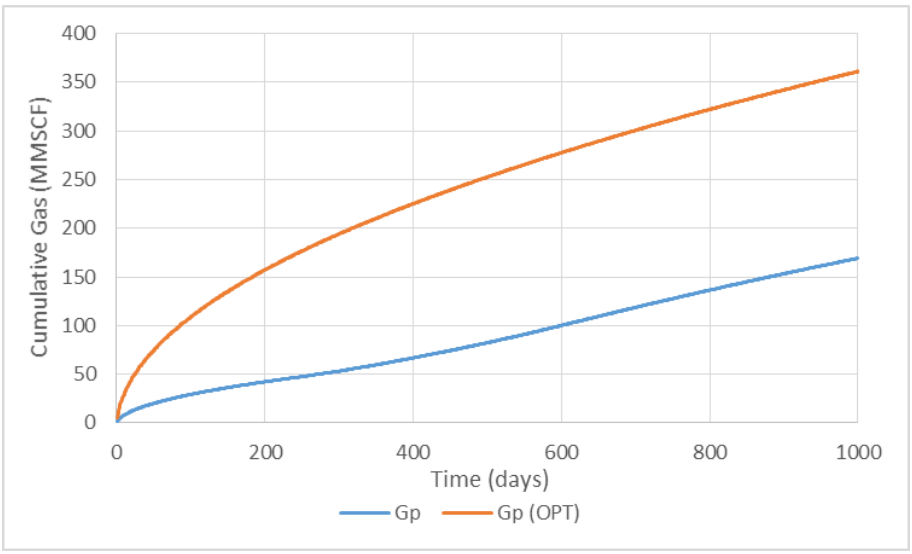

Figure 4.16. Cumulative gas comparison for case 4.

Figure 4.17 shows the comparison of cumulative condensate between initial well control and optimal well control. The final cumulative gas corresponding to the initial guess is 1.345 MSTB. The final cumulative condensate obtained with the optimal well control is 11.71189 MSTB, which is about 870.77% of the final cumulative condensate obtained with the initial well control.

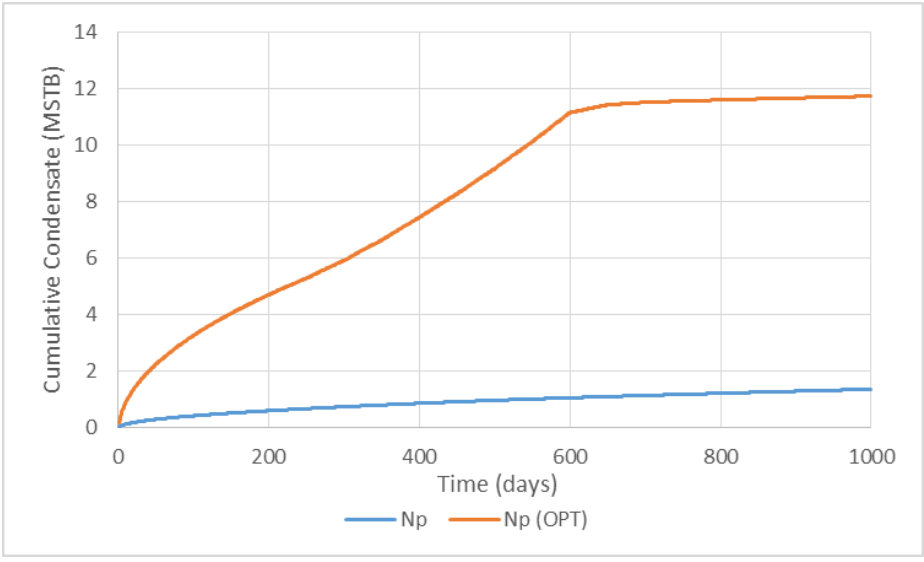

Figure 4.17. Cumulative condensate comparison for case 4.

Figure 4.18 shows the optimal well control. In this case, the optimal well control that leads to the maximum NPV stays slightly above 1000psi during the production.

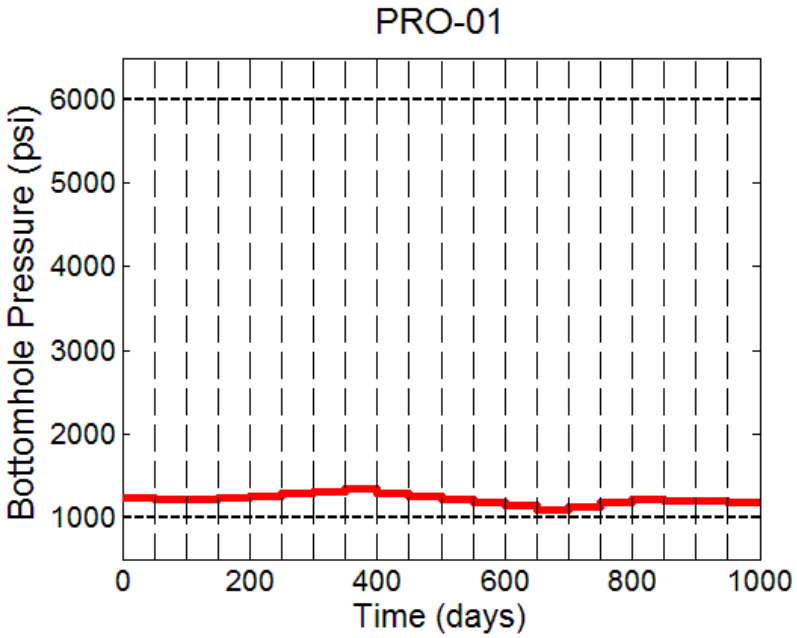

Figure 4.18. Optimal well control for case 4.

4.2.5 Case 5

In case 5, we use the corresponding R_v curve shown in light blue in Figure 4.2. Figure 4.19 shows the increase of NPV with respect to simulation numbers. The NPV obtained by the initial well setting is 1.1085 million dollars. Totally after 8 iterations (90 simulations), the final NPV is 2.2447 million dollars, which is about 2 times as much as the initial NPV. The total increase of NPV is 1.1362 million dollars. Figure 4.20 shows the comparison of cumulative gas between initial well control and optimal well control. The final cumulative gas corresponding to the initial guess is 183.66 MMscf. After optimization, the final cumulative gas is 376.40 MMscf, which is about 100% higher than the final cumulative gas obtained with the initial well control.

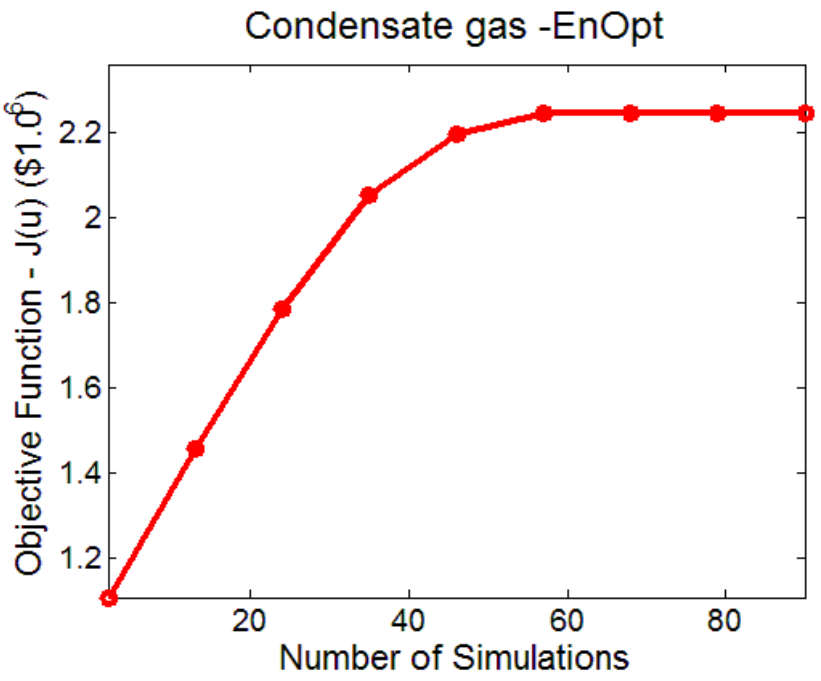

Figure 4.19. NPV vs. Numbers of simulations for case 5.

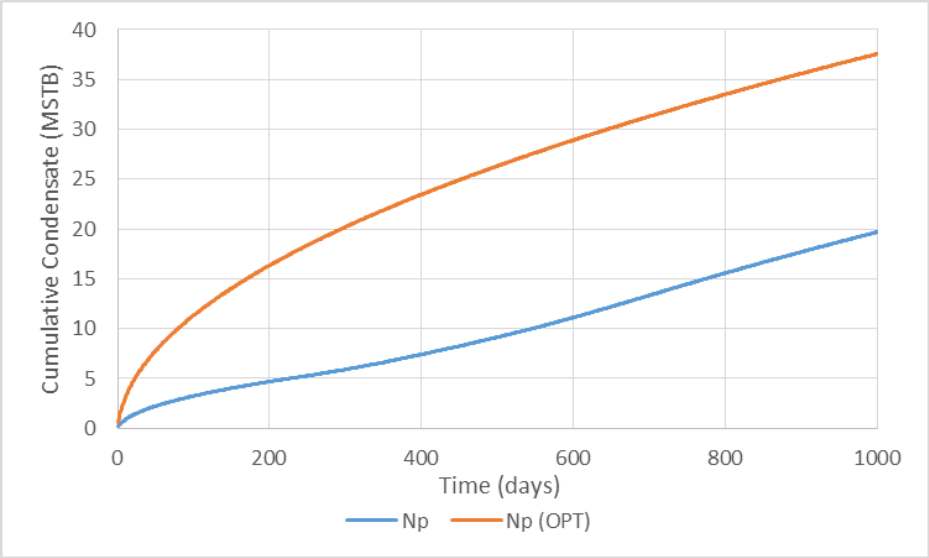

Figure 4.20. Cumulative gas comparison for case 5.

Figure 4.21 shows the comparison of cumulative condensate between initial well control and optimal well control. The final cumulative condensate corresponding to the

initial guess is 19.68 MSTB. The final cumulative condensate obtained with the optimal well control is 37.55 MSTB, which is about 91% higher than the final cumulative condensate obtained with the initial well control.

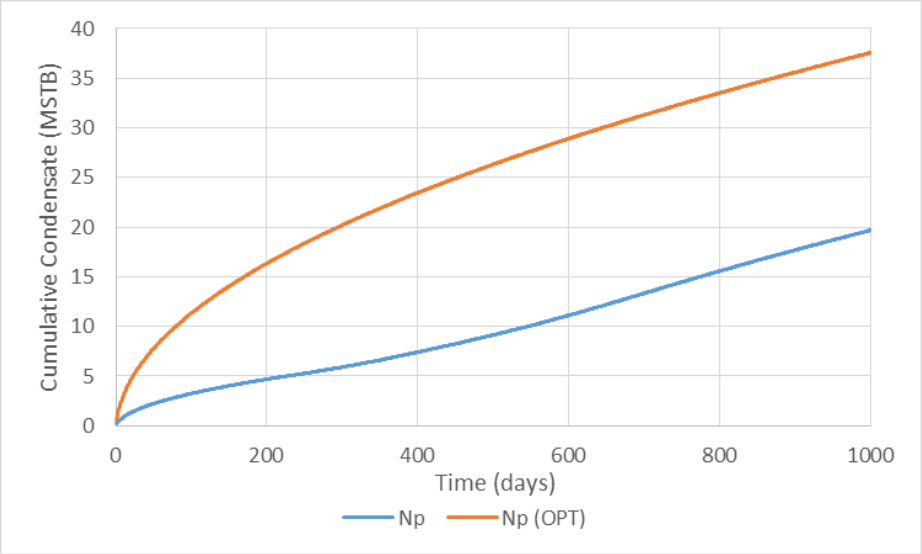

Figure 4.21. Cumulative condensate comparison for case 5.

Figure 4.22 shows the optimal well control for case 5. In this case, the optimal well control that leads to the maximum NPV stays right at 1000psi (lower boundary). As shown in Figure 4.2, as pressure decreases, the R_v value of case 5 does not change significantly after the dew point compared with case 4, but it changes rapidly below 1000 psi, which is the lower boundary. However, in case 4, the R_v value decreases gradually as the pressure drops. Therefore, in case 5, the optimal well schedule is when the BHP is at its minimum value.

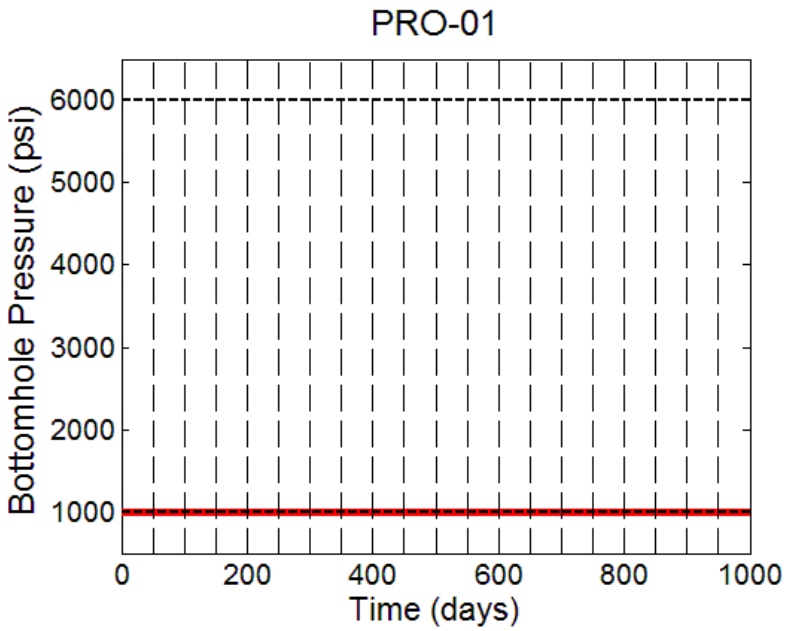

Figure 4.22. Optimal well control for case 5.

To investigate the effect of relative permeability on the optimal well schedule, we consider four cases with different oil and gas relative permeabilities by changing the exponents n_o and n_g in Corey's model (Eqns. 13 and 14). Figure 4.23 shows the oil and gas fractional flow curves corresponding to different relative permeabilities.

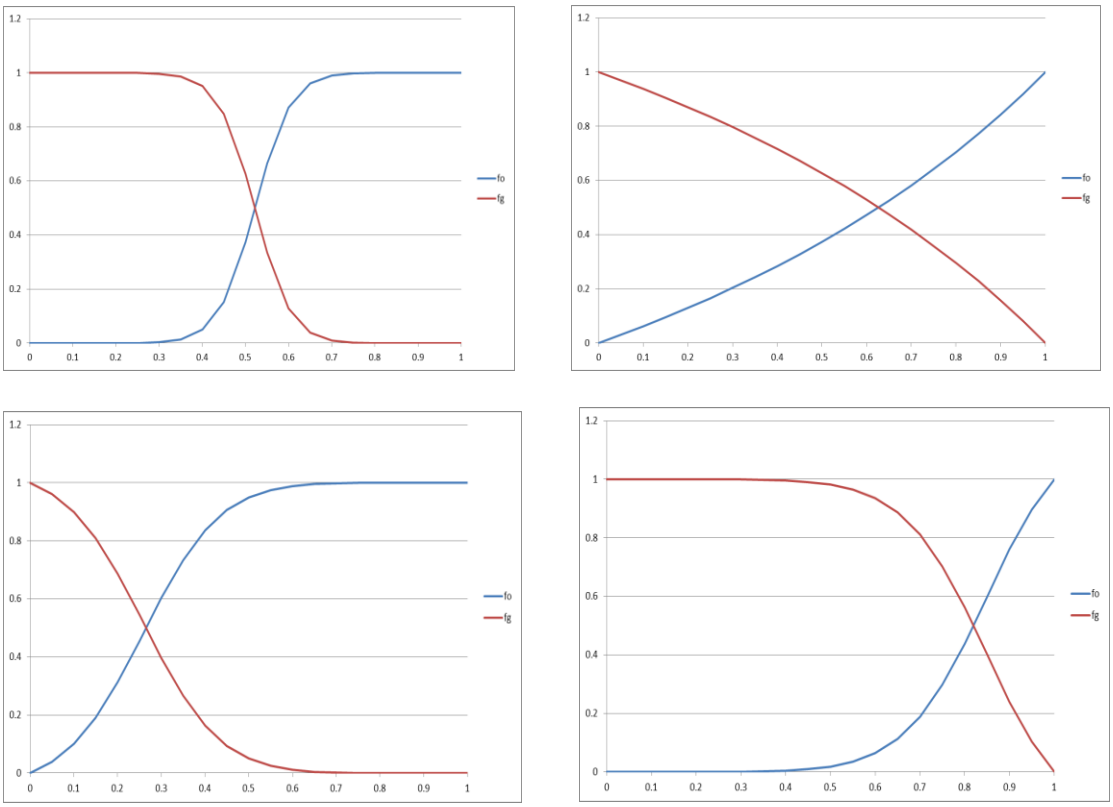

Figure 4.23. Oil and gas relative permeability curves.

After optimization, the results shown in Figure 4.24 demomstrate that the relative permeability does not have a significant impact on design of well schedule.

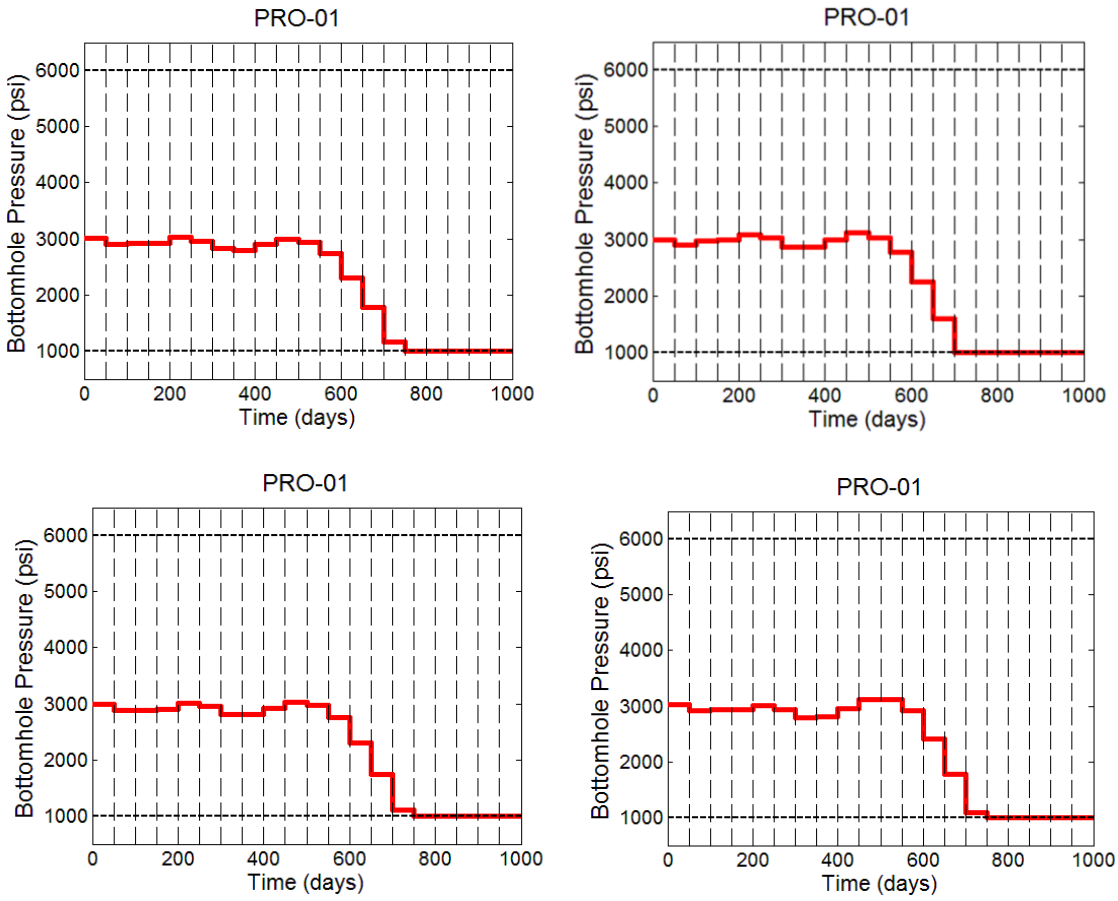

Figure 4.24. Optimal well control for cases with different relative permeabilities.

4.3 Summary

The study proves that the curvature of the R_v curve has a major impact on the optimal well schedule design. In particular, by comparing the results of the two extreme cases in Figures 4.6 and 4.22, we conclude that in cases with convex shaped R_v curves, the optimal well control is to hold the BHP at around the dew point for a while and drop it to the specified minimum BHP. On the other hand, in cases with concave shaped R_v curves, it is the best to directly drop the BHP at the beginning and hold the pressure at a relatively low value throughout the production.

CHAPTER 5

CONCLUSIONS

In this work, we implement a semi-analytical model derived from the dynamic drainage area (DDA) concept to forecast multi-fractured horizontal wells (MFHWs) completed in liquid-rich low-permeability reservoirs exhibiting two-phase flow of gas and oil/condensate. The accuracy of the new forecasting method is demonstrated through comparison of numerical simulation. The method is capable of handling different systems with either oil or gas as the primary phase. Also, it can deal with both transient linear flow regime and boundary dominated flow regime with varying flowing pressure.

The ES-MDA method is used to apply history matching to get a true reservoir description. Once a true reservoir description is available, we are able to implement the optimization algorithm to get the optimal well control which leads to maximum NPV. In this work, we use the stochastic smoothed Simplex method to optimize the well control. The study proves that the curvature of the R_v curve has a major impact on the optimal well schedule design. We conclude that in cases with convex shaped R_v curves, the optimal well control is to hold the BHP at around the dew point for a while and drop it to the specified minimum BHP. On the other hand, in cases with concave shaped R_v curves, it is the best to directly drop the BHP at the beginning and hold the pressure at a relatively low value throughout the production. However, the design of well schedule is not sensitive to relative permeability for condensate gas reservoirs.

BIBLIOGRAPHY

Alpak, F.O. and van Kats, F., 2009, January. Stochastic history matching of a deepwater turbidite reservoir. In SPE Reservoir Simulation Symposium. Society of Petroleum Engineers.

Sarma, P., Durlofsky, L.J., Aziz, K. and Chen, W.H., 2007, January. A new approach to automatic history matching using kernel PCA. In SPE Reservoir Simulation Symposium. Society of Petroleum Engineers.

Chen, W.H., Gavalas, G.R., Seinfeld, J.H., and Wasserman, M.L. 1974. A New Algorithm for Automatic History Matching. SPEJ 14 (6): 593-608. SPE-4545-PA.

Chavent, G.M., Dupuy, M., and Lemonnier, P. 1975. History Matching by Use of Optimal Control Theory. SPEJ 15 (1): 74-86. SPE-4627-PA.

Wasserman, M.L., Emanuel, A.S., and Seinfeld, J.H. 1975. Practical Applications of Optimal-Control Theory to History-Matching Multiphase Simulator Models. SPEJ 15 (4): 347-355. SPE-5020-PA.

Zhang, F. and Reynolds, A.C. 2002. Optimization Algorithms for Automatic History Matching of Production Data. Proc., 8th European Conference on the Mathematics of Oil Recovery, Freiberg, Germany.

Lee, T.Y. and Seinfeld, J.H. 1987. Estimation of Two-Phase Petroleum Reservoir Properties by Regularization. Journal of Computational Physics 69 (2): 397-419.

Olorode, O., Freeman, C.M., Moridis, G. et al. 2013. High-Resolution Numerical Modeling of Complex and Irregular Fracture Patterns in Shale-Gas Reservoirs and Tight Gas Reservoirs. DOI: 10.2118/152482-PA

H. Shojaei, E. S. Tajer, Analytical solution of transient multiphase flow to a horizontal well with multiple hydraulic fractures. SPE 165703, 2013.

Raghavan, R. and Joshi, S.D., 1993. Productivity of multiple drainholes or fractured horizontal wells. SPE formation evaluation, 8(01), pp.11-16.

Wei, Y. and Economides, M.J., 2005, January. Transverse hydraulic fractures from a horizontal well. In SPE Annual Technical Conference and Exhibition. Society of Petroleum Engineers.

Mukherjee, H. and Economides, M.J., 1991. A parametric comparison of horizontal and vertical well performance. SPE Formation Evaluation, 6(02), pp.209-216.

Guo, B., Yu, X. and Khoshgahdam, M., 2009. A simple analytical model for predicting productivity of multifractured horizontal wells. SPE reservoir evaluation & engineering, 12(06), pp.879-885.

Guo, G., Evans, R.D. and Chang, M.M., 1994, January. Pressure-transient behavior for a horizontal well intersecting multiple random discrete fractures. In SPE Annual Technical Conference and Exhibition. Society of Petroleum Engineers.

Ozkan, E. and Raghavan, R., 1991. New solutions for well-test-analysis problems: part 2 computational considerations and applications. SPE Formation Evaluation, 6(03), pp.369-378.

Raghavan, R.S., Chen, C.C. and Agarwal, B., 1997. An analysis of horizontal wells intercepted by multiple fractures. SPE Journal, 2(03), pp.235-245.

Brown, M., Ozkan, E., Raghavan, R. and Kazemi, H., 2011. Practical solutions for pressure-transient responses of fractured horizontal wells in unconventional shale reservoirs. SPE Reservoir Evaluation & Engineering, 14(06), pp.663-676.

Clarkson, C.R. and Qanbari, F., 2016. History Matching and Forecasting Tight Gas Condensate and Oil Wells by Use of an Approximate Semianalytical Model Derived From the Dynamic-Drainage-Area Concept. SPE Reservoir Evaluation & Engineering.

Erbas, D. and Christie, M.A., 2007, January. Effect of sampling strategies on prediction uncertainty estimation. In SPE Reservoir Simulation Symposium. Society of Petroleum Engineers.

Geophysical inversion with a neighbourhood algorithm—I. Searching a parameter space

Ouenes, A. and Saad, N., 1993, January. A new, fast parallel simulated annealing algorithm for reservoir characterization. In SPE Annual Technical Conference and Exhibition. Society of Petroleum Engineers.

Yang, N., Li, P. and Mei, B., 2007, August. An angle-based crossover tabu search for the traveling salesman problem. In Natural Computation, 2007. ICNC 2007. Third International Conference on (Vol. 4, pp. 512-516). IEEE.

Alpak, F.O. and van Kats, F., 2009, January. Stochastic history matching of a deepwater turbidite reservoir. In SPE Reservoir Simulation Symposium. Society of Petroleum Engineers.

Vazquez, M. and Beggs, H.D., 1980. Correlations for fluid physical property prediction.

Journal of Petroleum Technology, 32(06), pp.968-970.

Beggs, H.D. and Robinson, J.R., 1975. Estimating the viscosity of crude oil systems. Journal of Petroleum technology, 27(09), pp.1-140.